

Unifying aspects of light- and heavy-systems

Craig D. Roberts^{1,2}

¹ Physics Division, Bldg 203, Argonne National Laboratory
Argonne, Illinois 60439-4843, USA

² Fachbereich Physik, Universität Rostock, D-18051 Rostock, Germany

Abstract. Dyson-Schwinger equations furnish a Poincaré covariant framework within which to study hadrons. A particular feature is the existence of a nonperturbative, symmetry preserving truncation that enables the proof of exact results. Key to the DSE's efficacious application is their expression of the materially important momentum-dependent dressing of parton propagators at infrared length-scales, which is responsible for the magnitude of constituent-quark masses and the length-scale characterising confinement in bound states. A unified quantitative description of light- and heavy-quark systems is achieved by capitalising on these features.

1 Introduction

This contribution provides an overview of one particular means by which a quantitative and intuitive understanding of strong interaction phenomena can be attained. The broad framework is that of continuum strong QCD, by which I mean the continuum nonperturbative methods and models that can address these phenomena, especially those where a direct connection with QCD can be established, in one true limit or another. Naturally, everyone has a favourite tool and, in this connection, the Dyson-Schwinger equations (DSEs) are mine [1]. The framework is appropriate here because the last decade has seen a renaissance in its phenomenological application, with studies of phenomena as apparently unconnected as low-energy $\pi\pi$ scattering, $B \rightarrow D^*$ decays and the equation of state for a quark gluon plasma [2,3,4]. Indeed, the DSEs promise a single structure applicable to the gamut of strong interaction observables.

Dyson-Schwinger equations provide a nonperturbative means of analysing a quantum field theory. Derived from a theory's Euclidean space generating functional, they are an enumerable infinity of coupled integral equations whose solutions are the n -point Schwinger functions (Euclidean Green functions), which are the same matrix elements estimated in numerical simulations of lattice-QCD. In theories with elementary fermions, the simplest of the DSEs is the *gap* equation, which is basic to studying dynamical symmetry breaking in systems as disparate as ferromagnets, superconductors and QCD. The gap equation is a good example because it is familiar and has all the properties that characterise each DSE. Its solution is a 2-point function (the fermion propagator) but its kernel involves higher n -point functions; e.g., in a gauge theory, the kernel is constructed from the gauge-boson 2-point function and fermion-gauge-boson vertex, a 3-point function. In addition, while a weak-coupling expansion yields all the diagrams of perturbation theory, a self-consistent solution of the gap equation exhibits

nonperturbative effects unobtainable at any finite order in perturbation theory; e.g, dynamical chiral symmetry breaking (DCSB).

The coupling between equations; namely, the fact that the equation for a given m -point function always involves at least one $n > m$ -point function, necessitates a truncation of the tower of DSEs in order to define a tractable problem. It is unsurprising that the best known truncation scheme is just the weak coupling expansion which reproduces every diagram in perturbation theory. This scheme is systematic and valuable in the analysis of large momentum transfer processes because QCD is asymptotically free. However, it precludes the study of nonperturbative effects, and hence something else is needed for the investigation of strongly interacting systems and bound state phenomena.

In spite of the need for a truncation, gap equations have long been used effectively in obtaining nonperturbative information about many-body systems as, e.g., in the Nambu-Gorkov formalism for superconductivity. The positive outcomes have been achieved through the simple expedient of employing the most rudimentary truncation, e.g., Hartree or Hartree-Fock, and comparing the results with observations. Of course, agreement under these circumstances is not an unambiguous indication that the contributions omitted are small nor that the model expressed in the truncation is sound. However, it does justify further study, and an accumulation of good results is grounds for a concerted attempt to substantiate a reinterpretation of the truncation as the first term in a systematic and reliable approximation.

The modern application of DSEs, notably, comparisons with and predictions of experimental data, can properly be said to rest on model assumptions. However, those assumptions can be tested within the framework and also via comparison with lattice-QCD simulations, and the predictions are excellent. Furthermore, progress in understanding the intimate connection between symmetries and truncation schemes has enabled exact results to be proved. Herein I will briefly explain recent phenomenological applications and the foundation of their success, and focus especially on the links the approach provides between light- and heavy-quark phenomena. It will become apparent that the momentum-dependent *dressing* of the propagators of QCD's elementary excitations is a fundamental and observable feature of strong QCD.

The article is organised as follows: Sec. 2 [p. 3] – a review of DSE quiddities, especially in connection with the development of a nonperturbative, systematic and symmetry preserving truncation scheme, and the model-independent results whose proof its existence enables; Sec. 3 [p. 17] – an illustration of the efficacious application of DSE methods to light-meson systems and the connections that may be made with the results of lattice-QCD simulations; Sec. 4 [p. 23] – the natural extension of these methods to heavy-quark systems, with an explanation of the origin and derivation of heavy-quark symmetry limits and their confrontation with the real-world of finite quark masses; and Sec. 5 [p. 36] – an epilogue.

2 Dyson-Schwinger Equations

2.1 Gap Equation

The simplest DSE is the *gap* equation, which describes how the propagation of a fermion is modified by its interactions with the medium being traversed. In QCD that equation assumes the form:¹

$$S^{-1}(p) = Z_2(\zeta, \Lambda) i \gamma \cdot p + Z_4(\zeta, \Lambda) m(\zeta) + \Sigma'(p, \Lambda), \quad (1)$$

wherein the dressed-quark self-energy is

$$\Sigma'(p, \Lambda) = Z_1(\zeta, \Lambda) \int_q^{\Lambda} g^2 D_{\mu\nu}(p-q) \frac{\lambda^i}{2} \gamma_\mu S(q) \Gamma_\nu^i(q, p). \quad (2)$$

Equations (1), (2) constitute the renormalised DSE for the dressed-quark propagator. In Eq. (2), $D_{\mu\nu}(k)$ is the renormalised dressed-gluon propagator, $\Gamma_\nu^a(q; p)$ is the renormalised dressed-quark-gluon vertex and $\int_q^{\Lambda} := \int^{\Lambda} d^4q / (2\pi)^4$ represents a *translationally-invariant* regularisation of the integral, with Λ the regularisation mass-scale.² In addition, $Z_1(\zeta, \Lambda)$, $Z_2(\zeta, \Lambda)$ and $Z_4(\zeta, \Lambda)$ are, respectively, Lagrangian renormalisation constants for the quark-gluon vertex, quark wave function and quark mass-term, which depend on the renormalisation point, ζ , and the regularisation mass-scale, as does the gauge-independent mass renormalisation constant,

$$Z_m(\zeta^2, \Lambda^2) = Z_4(\zeta^2, \Lambda^2) Z_2^{-1}(\zeta^2, \Lambda^2), \quad (3)$$

whereby the renormalised running-mass is related to the bare mass:

$$m(\zeta) = Z_m^{-1}(\zeta^2, \Lambda^2) m_{\text{bm}}(\Lambda). \quad (4)$$

When ζ is very large the running-mass can be evaluated in perturbation theory, which gives

$$m(\zeta) = \frac{\hat{m}}{(\ln \zeta / \Lambda_{\text{QCD}})^{\gamma_m}}, \quad \gamma_m = 12 / (33 - 2N_f). \quad (5)$$

Here N_f is the number of current-quark flavours that contribute actively to the running coupling, and Λ_{QCD} and \hat{m} are renormalisation group invariants.

The solution of Eq. (1) is the dressed-quark propagator and takes the form

$$S^{-1}(p) = i\gamma \cdot p A(p^2, \zeta^2) + B(p^2, \zeta^2) \equiv \frac{1}{Z(p^2, \zeta^2)} [i\gamma \cdot p + M(p^2)]. \quad (6)$$

¹ A Euclidean metric is employed throughout, wherewith the scalar product of two four vectors is $a \cdot b = \sum_{i=1}^4 a_i b_i$; and I employ Hermitian Dirac- γ matrices that obey $\{\gamma_\mu, \gamma_\nu\} = 2\delta_{\mu\nu}$ and $\text{tr} \gamma_5 \gamma_\mu \gamma_\nu \gamma_\rho \gamma_\sigma = -4 \epsilon_{\mu\nu\rho\sigma}$, $\epsilon_{1234} = 1$.

² Only with a translationally invariant regularisation scheme can Ward-Takahashi identities be preserved, something that is crucial to ensuring vector and axial-vector current conservation. The final stage of any calculation is to take the limit $\Lambda \rightarrow \infty$.

It is obtained by solving the gap equation subject to the renormalisation condition that at some large spacelike ζ^2

$$S^{-1}(p)|_{p^2=\zeta^2} = i\gamma \cdot p + m(\zeta). \quad (7)$$

The observations made in in the Introduction are now manifest. The gap equation is a nonlinear integral equation for $S(p)$ and can therefore yield much-needed nonperturbative information. However, the kernel involves the two-point function $D_{\mu\nu}(k)$ and the three-point function $\Gamma_\nu^a(q;p)$. The equation is consequently coupled to the DSEs these functions satisfy and hence a manageable problem is obtained only once a truncation scheme is specified.

2.2 Nonperturbative Truncation

To understand why Eq. (1) is called a gap equation, consider the chiral limit, which is readily defined [5] because QCD exhibits asymptotic freedom and implemented in the gap equation by employing [6]

$$Z_2(\zeta^2, \Lambda^2) m_{\text{bm}}(\Lambda) \equiv 0, \quad \Lambda \gg \zeta. \quad (8)$$

It is noteworthy that for finite ζ and $\Lambda \rightarrow \infty$, the left hand side (l.h.s.) of Eq. (8) is identically zero, by definition, because the mass term in QCD's Lagrangian density is renormalisation-point-independent. The condition specified in Eq. (8), on the other hand, effects the result that at the (perturbative) renormalisation point there is no mass-scale associated with explicit chiral symmetry breaking, which is the essence of the chiral limit. An equivalent statement is that one obtains the chiral limit when the renormalisation-point-invariant current-quark mass vanishes; namely, $\hat{m} = 0$ in Eq. (5). In this case the theory is chirally symmetric, and a perturbative evaluation of the dressed-quark propagator from Eq. (1) gives

$$B_{\text{pert}}^0(p^2) := \lim_{m \rightarrow 0} B_{\text{pert}}(p^2) = \lim_{m \rightarrow 0} m \left(1 - \frac{\alpha}{\pi} \ln \left[\frac{p^2}{m^2} \right] + \dots \right) \equiv 0; \quad (9)$$

viz., the perturbative mass function is identically zero in the chiral limit. It follows that there is no gap between the top level in the quark's filled negative-energy Dirac sea and the lowest positive energy level.

However, suppose one has at hand a truncation scheme other than perturbation theory and that subject to this scheme Eq. (1) possessed a chiral limit solution $B^0(p^2) \neq 0$. Then interactions between the quark and the virtual quanta populating the ground state would have nonperturbatively generated a mass gap. The appearance of such a gap breaks the theory's chiral symmetry. This shows that the gap equation can be an important tool for studying DCSB, and it has long been used to explore this phenomenon in both QED and QCD [1].

The gap equation's kernel is formed from a product of the dressed-gluon propagator and dressed-quark-gluon vertex but in proposing and developing a truncation scheme it is insufficient to focus only on this kernel [6,7]. The gap

equation can only be a useful tool for studying DCSB if the truncation itself does not destroy chiral symmetry.

Chiral symmetry is expressed via the axial-vector Ward-Takahashi identity:

$$P_\mu \Gamma_{5\mu}(k; P) = S^{-1}(k_+) i\gamma_5 + i\gamma_5 S^{-1}(k_-), \quad k_\pm = k \pm P/2, \quad (10)$$

wherein $\Gamma_{5\mu}(k; P)$ is the dressed axial-vector vertex. This three-point function satisfies an inhomogeneous Bethe-Salpeter equation (BSE):

$$[\Gamma_{5\mu}(k; P)]_{tu} = Z_2 [\gamma_5 \gamma_\mu]_{tu} + \int_q^A [S(q_+) \Gamma_{5\mu}(q; P) S(q_-)]_{sr} K_{tu}^{rs}(q, k; P), \quad (11)$$

in which $K(q, k; P)$ is the fully-amputated quark-antiquark scattering kernel, and the colour-, Dirac- and flavour-matrix structure of the elements in the equation is denoted by the indices r, s, t, u . The Ward-Takahashi identity, Eq. (10), entails that an intimate relation exists between the kernel in the gap equation and that in the BSE. (This is another example of the coupling between DSEs.) Therefore an understanding of chiral symmetry and its dynamical breaking can only be obtained with a nonperturbative truncation scheme that preserves this relation, and hence guarantees Eq. (10) without a *fine-tuning* of model-dependent parameters.

Rainbow-ladder truncation. At least one such scheme exists [8]. Its leading-order term is the so-called renormalisation-group-improved rainbow-ladder truncation, whose analogue in the many body problem is an Hartree-Fock truncation of the one-body (Dyson) equation combined with a consistent ladder-truncation of the related two-body (Bethe-Salpeter) equation. To understand the origin of this leading-order term, observe that the dressed-ladder truncation of the quark-antiquark scattering kernel is expressed in Eq. (11) via

$$\begin{aligned} [L(q, k; P)]_{tu}^{t'u'} [\Gamma_{5\mu}(q; P)]_{u't'} &:= [S(q_+) \Gamma_{5\mu}(q; P) S(q_-)]_{sr} K_{tu}^{rs}(q, k; P) \\ &= -g^2 (\zeta^2) D_{\rho\sigma}(k - q) \\ &\quad \times [\Gamma_\rho^a(k_+, q_+) S(q_+)]_{tt'} [S(q_-) \Gamma_\sigma^a(q_-, k_-)]_{u'u} [\Gamma_{5\mu}(q; P)]_{t'u'} \end{aligned} \quad (12)$$

wherein I have only made explicit the renormalisation point dependence of the coupling. One can exploit multiplicative renormalisability and asymptotic freedom to demonstrate that on the kinematic domain for which $Q^2 := (k - q)^2 \sim k^2 \sim q^2$ is large and spacelike

$$[L(q, k; P)]_{tu}^{t'u'} = -4\pi\alpha(Q^2) D_{\rho\sigma}^{\text{free}}(Q) \left[\frac{\lambda^a}{2} \gamma_\rho S^{\text{free}}(q_+) \right]_{tt'} \left[S^{\text{free}}(q_-) \frac{\lambda^a}{2} \gamma_\sigma \right]_{u'u}, \quad (13)$$

where $\alpha(Q^2)$ is the strong running coupling and, e.g., S^{free} is the free quark propagator. It follows that on this domain the r.h.s. of Eq. (13) describes the leading contribution to the complete quark-antiquark scattering kernel, $K_{tu}^{rs}(q, k; P)$, with all other contributions suppressed by at least one additional power of $1/Q^2$.

The renormalisation-group-improved ladder-truncation supposes that

$$K_{tu}^{rs}(q, k; P) = -4\pi \alpha(Q^2) D_{\rho\sigma}^{\text{free}}(Q) \left[\frac{\lambda^a}{2} \gamma_\rho \right]_{ts} \left[\frac{\lambda^a}{2} \gamma_\sigma \right]_{ru} \quad (14)$$

is also a good approximation on the infrared domain and is thus an assumption about the long-range ($Q^2 \lesssim 1 \text{ GeV}^2$) behaviour of the interaction. Combining Eq. (14) with the requirement that Eq. (10) be automatically satisfied leads to the renormalisation-group-improved rainbow-truncation of the gap equation:

$$S^{-1}(p) = Z_2 (i\gamma \cdot p + m_{\text{bm}}) + \int_q^\Lambda 4\pi \alpha(Q^2) D_{\mu\nu}^{\text{free}}(p-q) \frac{\lambda^a}{2} \gamma_\mu S(q) \frac{\lambda^a}{2} \gamma_\nu. \quad (15)$$

This rainbow-ladder truncation provides the foundation for an explanation of a wide range of hadronic phenomena [4].

2.3 Systematic Procedure

The truncation scheme of Ref. [8] is a dressed-loop expansion of the dressed-quark-gluon vertices that appear in the half-amputated dressed-quark-antiquark scattering matrix: S^2K , a renormalisation-group invariant [9]. All n -point functions involved thereafter in connecting two particular quark-gluon vertices are *fully dressed*. The effect of this truncation in the gap equation, Eq. (1), is realised through the following representation of the dressed-quark-gluon vertex, $i\Gamma_\mu^a = \frac{i}{2} \lambda^a \Gamma_\mu = l^a \Gamma_\mu$:

$$\begin{aligned} Z_1 \Gamma_\mu(k, p) &= \gamma_\mu + \frac{1}{2N_c} \int_\ell^\Lambda g^2 D_{\rho\sigma}(p-\ell) \gamma_\rho S(\ell+k-p) \gamma_\mu S(\ell) \gamma_\sigma \\ &+ \frac{N_c}{2} \int_\ell^\Lambda g^2 D_{\sigma'\sigma}(\ell) D_{\tau'\tau}(\ell+k-p) \gamma_{\tau'} S(p-\ell) \gamma_{\sigma'} \Gamma_{\sigma\tau\mu}^{3g}(\ell, -k, k-p) + [\dots]. \end{aligned} \quad (16)$$

Here Γ^{3g} is the dressed-three-gluon vertex and it is readily apparent that the lowest order contribution to each term written explicitly is $\mathcal{O}(g^2)$. The ellipsis represents terms whose leading contribution is $\mathcal{O}(g^4)$; viz., the crossed-box and two-rung dressed-gluon ladder diagrams, and also terms of higher leading-order.

This expansion of S^2K , with its implications for other n -point functions, yields an ordered truncation of the DSEs that guarantees, term-by-term, the preservation of vector and axial-vector Ward-Takahashi identities, a feature that has been exploited [5,10,11] to establish exact results in QCD. It is readily seen that inserting Eq. (16) into Eq. (1) provides the rule by which the rainbow-ladder truncation can be systematically improved.

Planar vertex. The effect of the complete vertex in Eq. (16) on the solutions of the gap equation is unknown. However, insights have been drawn from a study

Fig. 1. Integral equation for a planar dressed-quark-gluon vertex obtained by neglecting contributions associated with explicit gluon self-interactions. Solid circles indicate fully dressed propagators. The vertices are not dressed. (Adapted from Ref. [9].)

[9] of a more modest problem obtained by retaining only the sum of dressed-gluon ladders; i.e., the vertex depicted in Fig. 1. The elucidation is particularly transparent when one employs [12]

$$\mathcal{D}_{\mu\nu}(k) := g^2 D_{\mu\nu}(k) = \left(\delta_{\mu\nu} - \frac{k_\mu k_\nu}{k^2} \right) (2\pi)^4 \mathcal{G}^2 \delta^4(k) \quad (17)$$

for the dressed-gluon line, which defines an ultraviolet finite model so that the regularisation mass-scale can be removed to infinity and the renormalisation constants set equal to one.³ This model has many positive features in common with the class of renormalisation-group-improved rainbow-ladder models and its particular momentum-dependence works to advantage in reducing integral equations to algebraic equations with similar qualitative features. There is naturally a drawback: the simple momentum dependence also leads to some model-dependent artefacts, but they are easily identified and hence not cause for concern.

The general form of the dressed-quark gluon vertex involves twelve distinct scalar form factors but using Eq. (17) only $\Gamma_\mu(p) := \Gamma_\mu(p, p)$ contributes to the gap equation, which considerably simplifies the analysis. The summation depicted in Fig. 1 is expressed via

$$\Gamma_\mu(p) = \gamma_\mu + \frac{1}{8} \gamma_\rho S(p) \Gamma_\mu(p) S(p) \gamma_\rho, \quad (18)$$

which supports a solution

$$\Gamma_\mu(p) = \alpha_1(p^2) \gamma_\mu + \alpha_2(p^2) \gamma \cdot p p_\mu - \alpha_3(p^2) i p_\mu. \quad (19)$$

One can re-express this vertex as

$$\Gamma_\mu(p) = \sum_{i=0}^{\infty} \Gamma_\mu^i(p) = \sum_{i=0}^{\infty} [\alpha_1^i(p^2) \gamma_\mu + \alpha_2^i(p^2) \gamma \cdot p p_\mu - \alpha_3^i(p^2) i p_\mu], \quad (20)$$

³ The constant \mathcal{G} sets the model's mass-scale and using $\mathcal{G} = 1$ simply means that all mass-dimensioned quantities are measured in units of \mathcal{G} .

where the superscript enumerates the order of the iterate: $\Gamma_\mu^{i=0}$ is the bare vertex,

$$\alpha_1^0 = 1, \quad \alpha_2^0 = 0 = \alpha_3^0; \quad (21)$$

$\Gamma_\mu^{i=1}$ is the result of inserting this into the r.h.s. of Eq (18) to obtain the one-rung dressed-gluon correction; $\Gamma_\mu^{i=2}$ is the result of inserting $\Gamma_\mu^{i=1}$, and is therefore the two-rung dressed-gluon correction; etc. A key observation [9] is that each iterate is related to its precursor via a simple recursion relation and, substituting Eq. (20), that recursion yields ($s = p^2$)

$$\boldsymbol{\alpha}^{i+1}(s) := \begin{pmatrix} \alpha_1^{i+1}(s) \\ \alpha_2^{i+1}(s) \\ \alpha_3^{i+1}(s) \end{pmatrix} = \mathcal{O}(s; A, B) \boldsymbol{\alpha}^i(s), \quad (22)$$

$$\mathcal{O}(s; A, B) = \frac{1}{4} \frac{1}{\Delta^2} \begin{pmatrix} -\Delta & 0 & 0 \\ 2A^2 & sA^2 - B^2 & 2AB \\ 4AB & 4sAB & 2(B^2 - sA^2) \end{pmatrix}, \quad (23)$$

$\Delta = sA^2(s) + B^2(s)$. It follows that

$$\boldsymbol{\alpha} = \left(\sum_{i=1}^{\infty} \mathcal{O}^i \right) \boldsymbol{\alpha}^0 = \frac{1}{1 - \mathcal{O}} \boldsymbol{\alpha}^0 \quad (24)$$

and hence, using Eq. (21),

$$\begin{aligned} \alpha_1 &= \frac{4\Delta}{1 + 4\Delta}, \\ \alpha_2 &= \frac{-8A^2}{1 + 2(B^2 - sA^2) - 8\Delta^2} \frac{1 + 2\Delta}{1 + 4\Delta}, \\ \alpha_3 &= \frac{-8AB}{1 + 2(B^2 - sA^2) - 8\Delta^2}. \end{aligned} \quad (25)$$

The recursion relation thus leads to a closed form for the gluon-ladder-dressed quark-gluon vertex in Fig. 1; viz., Eqs. (19), (25). Its momentum-dependence is determined by that of the dressed-quark propagator, which is obtained by solving the gap equation, itself constructed with this vertex. Using Eq. (17), that gap equation is

$$S^{-1}(p) = i\boldsymbol{\gamma} \cdot p + m + \gamma_\mu S(p) \Gamma_\mu(p) \quad (26)$$

whereupon the substitution of Eq. (19) gives

$$A(s) = 1 + \frac{1}{sA^2 + B^2} [A(2\alpha_1 - s\alpha_2) - B\alpha_3], \quad (27)$$

$$B(s) = m + \frac{1}{sA^2 + B^2} [B(4\alpha_1 + s\alpha_2) - sA\alpha_3]. \quad (28)$$

Equations (27), (28), completed using Eqs. (25), form a closed algebraic system. It can easily be solved numerically, and that yields simultaneously the complete

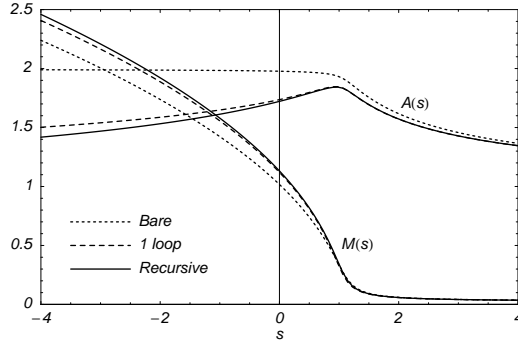


Fig. 2. $A(s)$, $M(s)$ obtained from Eqs. (25), (27), (28) with $m = 0.023$ (solid line). All dimensioned quantities are expressed in units of \mathcal{G} in Eq. (17). For comparison, the results obtained with the zeroth-order vertex (dotted line) and the one-loop vertex (dashed line) are also plotted. (Adapted from Ref. [9].)

gluon-ladder-dressed vertex and the propagator for a quark fully dressed via gluons coupling through this nonperturbative vertex. Furthermore, it is apparent that in the chiral limit, $m = 0$, a realisation of chiral symmetry in the Wigner-Weyl mode, which is expressed via the $B \equiv 0$ solution of the gap equation, is always admissible. This is the solution anticipated in Eq. (9).

The chiral limit gap equation also admits a Nambu-Goldstone mode solution whose $p^2 \simeq 0$ properties are unambiguously related to those of the $m \neq 0$ solution, a feature also evident in QCD [11]. A complete solution of Eq. (26) is available numerically, and results for the dressed-quark propagator are depicted in Fig. 2. It is readily seen that the complete resummation of dressed-gluon ladders gives a dressed-quark propagator that is little different from that obtained with the one-loop-corrected vertex; and there is no material difference from the result obtained using the zeroth-order vertex. Similar observations apply to the vertex itself. The scale of these modest effects can be quantified by a comparison between the values of $M(s=0) = B(0)/A(0)$ calculated using vertices dressed at different orders:

$$\frac{\sum_{i=0,N} \Gamma_{\mu}^i}{M(0)} \left\| \begin{array}{c|c|c|c} N=0 & N=1 & N=2 & N=\infty \\ \hline 1 & 1.105 & 1.115 & 1.117 \end{array} \right. \quad (29)$$

The rainbow truncation of the gap equation is accurate to within 12% and adding just one gluon ladder gives 1% accuracy. It is important to couple this with an understanding of how the vertex resummation affects the Bethe-Salpeter kernel.

Vertex-consistent Bethe-Salpeter kernel. The renormalised homogeneous BSE for the quark-antiquark channel denoted by M can be expressed

$$[\Gamma_M(k; P)]_{tu} = \int_q^{\Lambda} [\chi_M(q; P)]_{sr} [K(k, q; P)]_{tu}^{rs}, \quad (30)$$

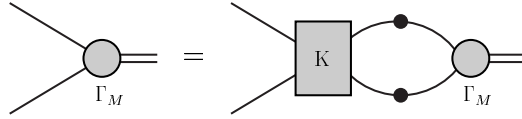


Fig. 3. Homogeneous BSE, Eq. (30). Filled circles: dressed propagators or vertices; K is the dressed-quark-antiquark scattering kernel. A systematic truncation of $S^2 K$ is the key to preserving Ward-Takahashi identities [8,14]. (Adapted from Ref. [9].)

where: $\Gamma_M(k; P)$ is the meson's Bethe-Salpeter amplitude, k is the relative momentum of the quark-antiquark pair, P is their total momentum; and

$$\chi_M(k; P) = S(k_+) \Gamma_M(k; P) S(k_-). \quad (31)$$

Equation (30), depicted in Fig. 3, describes the residue at a pole in the solution of an inhomogeneous BSE; e.g., the lowest mass pole solution of Eq. (11) is identified with the pion.⁴

I noted on p. 5 that the automatic preservation of Ward-Takahashi identities in those channels related to strong interaction observables requires a conspiracy between the dressed-quark-gluon vertex and the Bethe-Salpeter kernel [8,14]. A systematic procedure for building that kernel follows [9] from the observation [14] that the gap equation can be expressed via

$$\frac{\delta \Gamma[S]}{\delta S} = 0, \quad (32)$$

where $\Gamma[S]$ is a Cornwall-Jackiw-Tomboulis-like effective action [15]. The Bethe-Salpeter kernel is then obtained via an additional functional derivative:

$$K_{tu}^{rs} = -\frac{\delta \Sigma_{tu}}{\delta S_{rs}}. \quad (33)$$

With the vertex depicted in Fig. 1, the n -th order contribution to the kernel is obtained from the n -loop contribution to the self energy:

$$\Sigma^n(p) = -\int_q^\Lambda \mathcal{D}_{\mu\nu}(p-q) l^a \gamma_\mu S(q) l^a \Gamma_\nu^n(q, p). \quad (34)$$

Since $\Gamma_\mu(p, q)$ itself depends on S then Eq. (33) yields the Bethe-Salpeter kernel as a sum of two terms and hence Eq. (30) assumes the form

$$\Gamma_M(k; P) = \int_q^\Lambda \mathcal{D}_{\mu\nu}(k-q) l^a \gamma_\mu \left[\chi_M(q; P) l^a \Gamma_\nu(q_-, k_-) + S(q_+) \Lambda_{M\nu}^a(q, k; P) \right], \quad (35)$$

⁴ The canonical normalisation of a Bethe-Salpeter amplitude is fixed by requiring that the bound state contribute with unit residue to the fully-amputated quark-antiquark scattering amplitude: $M = K + K(SS)K + [\dots]$. See, e.g., Ref. [13].

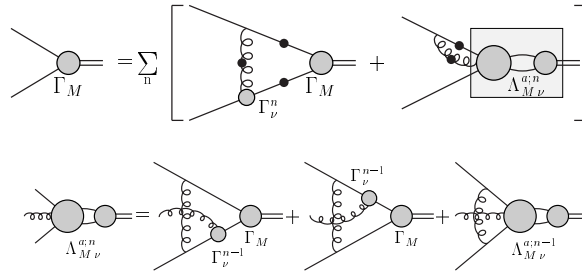


Fig. 4. Upper panel: BSE, Eq. (35), which is valid whenever Γ_μ can be obtained via a recursion relation. Lower panel: Recursion relation for $\Lambda_{M\nu}^{\alpha;n}$. (Adapted from Ref. [9].)

where I have used the mnemonic

$$\Lambda_{M\nu}^\alpha(q, k; P) = \sum_{n=0}^{\infty} \Lambda_{M\nu}^{\alpha;n}(q, k; P). \quad (36)$$

Equation (35) is depicted in the upper panel of Fig. 4. The first term is instantly available once one has an explicit form for Γ_ν^n and the second term, identified by the shaded box in Fig. 4, can be obtained [9] via the inhomogeneous recursion relation depicted in the figure's lower panel. Combining these figures, it is apparent that to form the Bethe-Salpeter kernel the free gluon line is attached to the upper dressed-quark line. Consequently, the first term on the r.h.s. of the lower panel in Fig. 4 invariably generates crossed gluon lines; viz., nonplanar contributions to the kernel. The character of the vertex-consistent Bethe-Salpeter kernel is now clear: it consists of countably many contributions, a subclass of which are crossed-ladder diagrams and hence nonplanar. Only the rainbow gap equation, obtained with $i = 0$ in Eq. (20), yields a planar vertex-consistent Bethe-Salpeter kernel, namely the ladder kernel of Eq. (14). In this case alone is the number of diagrams in the dressed-vertex and kernel identical. Otherwise there are always more terms in the kernel.

Solutions for the π - and ρ -mesons. I have recapitulated on a general procedure that provides the vertex-consistent channel-projected Bethe-Salpeter kernel once Γ_ν^n and the propagator functions; A , B , are known. That kernel must be constructed independently for each channel because, e.g., $\Lambda_{M\nu}^\alpha$ depends on $\chi_M(q; P)$. As with the study of the vertex, an elucidation of the resulting BSEs' features is simplified by using the model of Eq. (17), for then the Bethe-Salpeter kernels are finite matrices [cf. $(1 - \mathcal{O})^{-1}$ in Eq. (24)] and the homogeneous BSEs are merely linear, coupled algebraic equations.

Reference [9] describes in detail the solution of the coupled gap and Bethe-Salpeter equations for the π - and ρ -mesons. Herein I focus on the results, which are summarised in Table 1. It is evident that, irrespective of the order of the truncation; viz., the number of dressed gluon rungs in the quark-gluon vertex, the

Table 1. Calculated π and ρ meson masses, in GeV, quoted with $\mathcal{G} = 0.48$ GeV, in which case $m = 0.023 \mathcal{G} = 11$ MeV. n is the number of dressed-gluon rungs retained in the planar vertex, see Fig. 1, and hence the order of the vertex-consistent Bethe-Salpeter kernel: the rapid convergence of the kernel is apparent from the tabulated results. (Adapted from Ref. [9].)

	$M_H^{n=0}$	$M_H^{n=1}$	$M_H^{n=2}$	$M_H^{n=\infty}$
$\pi, m = 0$	0	0	0	0
$\pi, m = 0.011$	0.152	0.152	0.152	0.152
$\rho, m = 0$	0.678	0.745	0.754	0.754
$\rho, m = 0.011$	0.695	0.762	0.770	0.770

pion is massless in the chiral limit. This is in spite of the fact that it is composed of heavy dressed-quarks, as is clear in the calculated scale of the dynamically generated dressed-quark mass function: see Fig. 2, $M(0) \approx \mathcal{G} \approx 0.5$ GeV. These observations emphasise that the masslessness of the π is a model-independent consequence of consistency between the Bethe-Salpeter kernel and the kernel in the gap equation. Furthermore, the bulk of the ρ - π mass splitting is present for $m = 0$ and with the simplest ($n = 0$; i.e., rainbow-ladder) kernel, which demonstrates that this mass difference is driven by the DCSB mechanism. It is not the result of a carefully contrived chromo-hyperfine interaction. Finally, the quantitative effect of improving on the rainbow-ladder truncation; namely, including more dressed-gluon rungs in the gap equation's kernel and consistently improving the kernel in the Bethe-Salpeter equation, is a 10% correction to the vector meson mass. Simply including the first correction (viz., retaining the first two diagrams in Fig. 1) yields a vector meson mass that differs from the fully resummed result by $\approx 1\%$. The rainbow-ladder truncation is clearly accurate in these channels.

Comments. While I have described results obtained with a rudimentary interaction model in order to make the construction transparent, the procedure is completely general. However, the algebraic simplicity of the analysis is naturally peculiar to the model. With a more realistic interaction, the gap and vertex equations yield a system of twelve coupled integral equations. The Bethe-Salpeter kernel for any given channel then follows as the solution of a determined integral equation.

The material reviewed covers those points in the construction of Refs. [8,9] that bear upon the fidelity of the rainbow-ladder truncation in pairing the gap equation and Bethe-Salpeter equations for the vector and flavour non-singlet pseudoscalar mesons. The error is small. In modelling it is therefore justified to fit one's parameters to physical observables at this level in these channels and then make predictions for other phenomena involving vector and pseudoscalar

bound states in the expectation they will be reliable. That approach has been successful, as illustrated in Ref. [4].

Lastly, the placement of the rainbow-ladder truncation as the first term in a procedure that can methodically be improved explains why this truncation has been successful, the boundaries of its success, why it has failed outside these boundaries, and why sorting out the failures won't undermine the successes.

2.4 Selected Model-Independent Results

In the hadron spectrum the pion is identified as both a Goldstone mode, associated with DCSB, and a bound state composed of constituent u - and d -quarks, whose effective mass is $\sim 300 - 500$ MeV. Naturally, in quantum mechanics, one can fabricate a mass operator that yields a bound state whose mass is much less than the sum of the constituents' masses. However, that requires *fine tuning* and, without additional fine tuning, such models predict properties for spin- and/or isospin-flip relatives of the pion which conflict with experiment. A correct resolution of this apparent dichotomy is one of the fundamental challenges to establishing QCD as the theory underlying strong interaction physics, and the DSEs provide an ideal framework within which to achieve that end, as I now explain following the proof of Ref. [5]. It cannot be emphasised too strongly that the legitimate understanding of pion observables; including its mass, decay constant and form factors, requires an approach to contain a well-defined and valid chiral limit.

Proof of Goldstone's Theorem. Consider the BSE expressed for the isovector pseudoscalar channel:

$$[\Gamma_\pi^j(k; P)]_{tu} = \int_q^\Lambda [\chi_\pi^j(q; P)]_{sr} K_{tu}^{rs}(q, k; P), \quad (37)$$

with $\chi_\pi^j(q; P) = S(q_+) \Gamma_\pi^j(q; P) S(q_-)$ obvious from Eq. (31) and j labelling isospin, of which the solution has the general form

$$\begin{aligned} \Gamma_\pi^j(k; P) = \tau^j \gamma_5 \left[i E_\pi(k; P) + \gamma \cdot P F_\pi(k; P) \right. \\ \left. + \gamma \cdot k k \cdot P G_\pi(k; P) + \sigma_{\mu\nu} k_\mu P_\nu H_\pi(k; P) \right]. \end{aligned} \quad (38)$$

It is apparent that the dressed-quark propagator, the solution of Eq. (1), is an important part of the BSE's kernel.

Chiral symmetry and its dynamical breaking are expressed in the axial-vector Ward-Takahashi identity, Eq. (10), which involves the axial-vector vertex:

$$[\Gamma_{5\mu}^j(k; P)]_{tu} = Z_2 \left[\gamma_5 \gamma_\mu \frac{\tau^j}{2} \right]_{tu} + \int_q^\Lambda [\chi_{5\mu}^j(q; P)]_{sr} K_{tu}^{rs}(q, k; P), \quad (39)$$

that has the general form

$$\begin{aligned} \Gamma_{5\mu}^j(k; P) &= \frac{\tau^j}{2} \gamma_5 [\gamma_\mu F_R(k; P) + \gamma \cdot k k_\mu G_R(k; P) - \sigma_{\mu\nu} k_\nu H_R(k; P)] \\ &\quad + \tilde{\Gamma}_{5\mu}^j(k; P) + \frac{P_\mu}{P^2 + m_\phi^2} \phi^j(k; P), \end{aligned} \quad (40)$$

where F_R , G_R , H_R and $\tilde{\Gamma}_{5\mu}^i$ are regular as $P^2 \rightarrow -m_\phi^2$, $P_\mu \tilde{\Gamma}_{5\mu}^i(k; P) \sim \mathcal{O}(P^2)$ and $\phi^j(k; P)$ has the structure depicted in Eq. (38). Equation (40) admits the possibility of at least one pole term in the vertex but does not require it.

Substituting Eq. (40) into (39) and equating putative pole terms, it is clear that, if present, $\phi^j(k; P)$ satisfies Eq. (37). Since this is an eigenvalue problem that only admits a $\Gamma_\pi^j \neq 0$ solution for $P^2 = -m_\pi^2$, it follows that $\phi^j(k; P)$ is nonzero solely for $P^2 = -m_\pi^2$ and the pole mass is $m_\phi^2 = m_\pi^2$. Hence, if K supports such a bound state, the axial-vector vertex contains a pion-pole contribution. Its residue, r_A , however, is not fixed by these arguments. Thus Eq. (40) becomes

$$\begin{aligned} \Gamma_{5\mu}^j(k; P) &= \frac{\tau^j}{2} \gamma_5 [\gamma_\mu F_R(k; P) + \gamma \cdot k k_\mu G_R(k; P) - \sigma_{\mu\nu} k_\nu H_R(k; P)] \\ &\quad + \tilde{\Gamma}_{5\mu}^i(k; P) + \frac{r_A P_\mu}{P^2 + m_\pi^2} \Gamma_\pi^j(k; P). \end{aligned} \quad (41)$$

Consider now the chiral limit axial-vector Ward-Takahashi identity, Eq. (10). If one assumes $m_\pi^2 = 0$ in Eq. (41), substitutes it into the l.h.s. of Eq. (10) along with Eq. (6) on the right, and equates terms of order $(P_\nu)^0$ and P_ν , one obtains the chiral-limit relations [5]

$$\begin{aligned} r_A E_\pi(k; 0) &= B(k^2), & F_R(k; 0) + 2r_A F_\pi(k; 0) &= A(k^2), \\ G_R(k; 0) + 2r_A G_\pi(k; 0) &= 2A'(k^2), & H_R(k; 0) + 2r_A H_\pi(k; 0) &= 0. \end{aligned} \quad (42)$$

I have already explained that $B(k^2) \equiv 0$ in the chiral limit [remember Eq. (9)] and that a $B(k^2) \neq 0$ solution of Eq. (1) in the chiral limit signals DCSB. Indeed, in this case [16]

$$M(p^2) \stackrel{\text{large-}p^2}{\equiv} \frac{2\pi^2 \gamma_m}{3} \frac{(-\langle \bar{q}q \rangle^0)}{p^2 \left(\frac{1}{2} \ln \left[p^2 / \Lambda_{\text{QCD}}^2 \right] \right)^{1-\gamma_m}}, \quad (43)$$

where $\langle \bar{q}q \rangle^0$ is the renormalisation-point-independent vacuum quark condensate [17]. Furthermore, there is at least one nonperturbative DSE truncation scheme that preserves the axial-vector Ward-Takahashi identity, order by order. Hence Eqs. (42) are exact quark-level Goldberger-Treiman relations, which state that when chiral symmetry is dynamically broken:

- (i). the homogeneous isovector pseudoscalar BSE has a massless solution;
- (ii). the Bethe-Salpeter amplitude for the massless bound state has a term proportional to γ_5 alone, with $E_\pi(k; 0)$ completely determined by the scalar part of the quark self energy, in addition to other pseudoscalar Dirac structures, F_π , G_π and H_π , that are nonzero;
- (iii). and the axial-vector vertex is dominated by the pion pole for $P^2 \simeq 0$.

The converse is also true. Hence DCSB is a sufficient and necessary condition for the appearance of a massless pseudoscalar bound state (of what can be very-massive constituents) that dominates the axial-vector vertex for $P^2 \approx 0$.

Mass Formula. When chiral symmetry is explicitly broken the axial-vector Ward-Takahashi identity becomes:

$$P_\mu \Gamma_{5\mu}^j(k; P) = S^{-1}(k_+) i\gamma_5 \frac{\tau^j}{2} + i\gamma_5 \frac{\tau^j}{2} S^{-1}(k_-) - 2i m(\zeta) \Gamma_5^j(k; P), \quad (44)$$

where the pseudoscalar vertex is obtained from

$$\left[\Gamma_5^j(k; P) \right]_{tu} = Z_4 \left[\gamma_5 \frac{\tau^j}{2} \right]_{tu} + \int_q^A \left[\chi_5^j(q; P) \right]_{sr} K_{tu}^{rs}(q, k; P). \quad (45)$$

As argued in connection with Eq. (39), the solution of Eq. (45) has the form

$$\begin{aligned} i\Gamma_5^j(k; P) = & \frac{\tau^j}{2} \gamma_5 \left[iE_R^P(k; P) + \gamma \cdot P F_R^P + \gamma \cdot k k \cdot P G_R^P(k; P) \right. \\ & \left. + \sigma_{\mu\nu} k_\mu P_\nu H_R^P(k; P) \right] + \frac{r_P}{P^2 + m_\pi^2} \Gamma_\pi^j(k; P), \end{aligned} \quad (46)$$

where E_R^P , F_R^P , G_R^P and H_R^P are regular as $P^2 \rightarrow -m_\pi^2$; i.e., the isovector pseudoscalar vertex also receives a contribution from the pion pole. In this case equating pole terms in the Ward-Takahashi identity, Eq. (44), entails [5]

$$r_A m_\pi^2 = 2 m(\zeta) r_P(\zeta). \quad (47)$$

This, too, is an exact relation in QCD. Now it is important to determine the residues r_A and r_P .

Study of the renormalised axial-vector vacuum polarisation shows [5]:

$$r_A \delta^{ij} P_\mu = f_\pi \delta^{ij} P_\mu = Z_2 \text{tr} \int_q^A \frac{1}{2} \tau^i \gamma_5 \gamma_\mu S(q_+) \Gamma_\pi^j(q; P) S(q_-), \quad (48)$$

where the trace is over colour, Dirac and flavour indices; i.e., the residue of the pion pole in the axial-vector vertex is the pion decay constant. The factor of Z_2 on the r.h.s. in Eq. (48) is crucial: it ensures the result is gauge invariant, and cutoff and renormalisation-point independent. Equation (48) is the exact expression in quantum field theory for the pseudovector projection of the pion's wave function on the origin in configuration space.

A close inspection of Eq. (45), following its re-expression in terms of the renormalised, fully-amputated quark-antiquark scattering amplitude: $M = K + K(SS)K + \dots$, yields [5]

$$i r_P \delta^{ij} = Z_4 \text{tr} \int_q^A \frac{1}{2} \tau^i \gamma_5 S(q_+) \Gamma_\pi^j(q; P) S(q_-), \quad (49)$$

wherein the dependence of Z_4 on the gauge parameter, the regularisation mass-scale and the renormalisation point is exactly that required to ensure: 1) r_P is finite in the limit $\Lambda \rightarrow \infty$; 2) r_P is gauge-parameter independent; and 3) the renormalisation point dependence of r_P is just such as to guarantee the r.h.s. of Eq. (47) is renormalisation point *independent*. Equation (49) expresses the pseudoscalar projection of the pion's wave function on the origin in configuration space.

Focus for a moment on the chiral limit behaviour of Eq. (49) whereat, using Eqs. (38), (42), one finds readily

$$-\langle \bar{q}q \rangle_\zeta^0 = f_\pi r_P^0(\zeta) = Z_4(\zeta, \Lambda) N_c \text{tr}_D \int_q^\Lambda S_{\hat{m}=0}(q). \quad (50)$$

Equation (50) is unique as the expression for the chiral limit *vacuum quark condensate*.⁵ It is ζ -dependent but independent of the gauge parameter and the regularisation mass-scale, and Eq. (50) thus proves that the chiral-limit residue of the pion pole in the pseudoscalar vertex is $(-\langle \bar{q}q \rangle_\zeta^0)/f_\pi$. Now Eqs. (47), (50) yield

$$(f_\pi^0)^2 m_\pi^2 = -2 m(\zeta) \langle \bar{q}q \rangle_\zeta^0 + \text{O}(\hat{m}^2), \quad (51)$$

where f_π^0 is the chiral limit value from Eq. (48). Hence what is commonly known as the Gell-Mann–Oakes–Renner relation is a *corollary* of Eq. (47).

One can now understand the results in Table 1: a massless bound state of massive constituents is a necessary consequence of DCSB and will emerge in any few-body approach to QCD that employs a systematic truncation scheme which preserves the Ward-Takahashi identities.

Upon review it will be apparent that Eqs. (47) – (49) are valid for any values of the current-quark masses, and the generalisation to N_f quark flavours is [6,10,11]

$$f_H^2 m_H^2 = -\langle \bar{q}q \rangle_\zeta^H \mathcal{M}_H^\zeta, \quad (52)$$

$\mathcal{M}_H^\zeta = m_{q_1}^\zeta + m_{q_2}^\zeta$ is the sum of the current-quark masses of the meson's constituents;

$$f_H P_\mu = Z_2 \text{tr} \int_q^\Lambda \frac{1}{2} (T^H)^T \gamma_5 \gamma_\mu \mathcal{S}(q_+) \Gamma^H(q; P) \mathcal{S}(q_-), \quad (53)$$

with $\mathcal{S} = \text{diag}(S_u, S_d, S_s, \dots)$, T^H a flavour matrix specifying the meson's quark content, e.g., $T^{\pi^+} = \frac{1}{2}(\lambda^1 + i\lambda^2)$, $\{\lambda^i\}$ are N_f -flavour generalisations of the Gell-Mann matrices; and

$$\langle \bar{q}q \rangle_\zeta^H = -f_H r_H^\zeta = i f_H Z_4 \text{tr} \int_q^\Lambda \frac{1}{2} (T^H)^T \gamma_5 \mathcal{S}(q_+) \Gamma^H(q; P) \mathcal{S}(q_-). \quad (54)$$

NB. Equation (50) means that in the chiral limit $\langle \bar{q}q \rangle_\zeta^H \rightarrow \langle \bar{q}q \rangle_\zeta^0$ and hence $\langle \bar{q}q \rangle_\zeta^H$ has been called an *in-hadron condensate*.

⁵ The trace of the massive dressed-quark propagator is not renormalisable and hence there is no unique definition of a massive-quark condensate [17].

The formulae reviewed in this Section also yield model-independent corollaries for systems involving heavy-quarks, as I relate in Sec. 4.

3 Basis for a Description of Mesons

The renormalisation-group-improved rainbow-ladder truncation has long been employed to study light mesons, and in Secs. 2.2, 2.3 it was shown to be a quantitatively reliable tool for vector and flavour nonsinglet pseudoscalar mesons. In connection with Eqs. (14), (15), I argued that the truncation preserves the ultra-violet behaviour of the quark-antiquark scattering kernel in QCD but requires an assumption about that kernel in the infrared; viz., on the domain $Q^2 \lesssim 1 \text{ GeV}^2$, which corresponds to length-scales $\gtrsim 0.2 \text{ fm}$. The calculation of this behaviour is a primary challenge in contemporary hadron physics and there is progress [7,18,19,20,21,22,23]. However, at present the most efficacious approach is to model the kernel in the infrared, which enables quantitative comparisons with experiments that can be used to inform theoretical analyses. The most extensively applied model is specified by [24]

$$\frac{\alpha(Q^2)}{Q^2} = \frac{4\pi^2}{\omega^6} D Q^2 e^{-Q^2/\omega^2} + \frac{8\pi^2 \gamma_m}{\ln \left[\tau + \left(1 + Q^2/\Lambda_{\text{QCD}}^2 \right)^2 \right]} \mathcal{F}(Q^2), \quad (55)$$

in Eqs. (14), (15). Here, $\mathcal{F}(Q^2) = [1 - \exp(-Q^2/[4m_t^2])]/Q^2$, $m_t = 0.5 \text{ GeV}$; $\tau = e^2 - 1$; $\gamma_m = 12/25$; and [25] $\Lambda_{\text{QCD}} = \Lambda_{\text{MS}}^{(4)} = 0.234 \text{ GeV}$. This simple form expresses the interaction strength as a sum of two terms: the second ensures that perturbative behaviour is preserved at short-range; and the first makes provision for the possibility of enhancement at long-range. The true parameters in Eq. (55) are D and ω , which together determine the integrated infrared strength of the rainbow-ladder kernel; i.e., the so-called interaction tension, σ^Δ [18]. However, I emphasise that they are not independent: in fitting to a selection of observables, a change in one is compensated by altering the other; e.g., on the domain $\omega \in [0.3, 0.5] \text{ GeV}$, the fitted observables are approximately constant along the trajectory [7]

$$\omega D = (0.72 \text{ GeV})^3. \quad (56)$$

Hence Eq. (55) is a one-parameter model. This correlation: a reduction in D compensating an increase in ω , ensures a fixed value of the interaction tension.

3.1 Rainbow Gap Equation

Equations (15) and (55) provide a model for QCD's gap equation and in hadron physics applications one is naturally interested in the nonperturbative DCSB solution. A familiar property of gap equations is that they only support such a solution if the interaction tension exceeds some critical value. In the present case that value is $\sigma_c^\Delta \sim 2.5 \text{ GeV/fm}$ [18]. This amount of infrared strength is sufficient to generate a nonzero vacuum quark condensate *but only just*. An acceptable

Table 2. Comparison of experimental values with results for π and K observables calculated using the rainbow-ladder interaction specified by Eq. (55), quoted in MeV. The model’s sole parameter and the current-quark masses were varied to obtain these results, and the best fit parameter values are given in Eqs. (57), (58). Predictions for analogous vector meson observables are also tabulated. NB. A charged particle normalisation is used for f_H^V in Eq. (61), which differs from that in Eq. (53) by a multiplicative factor of $\sqrt{2}$. (Adapted from Ref. [24].)

	m_π	m_K	f_π	f_K	m_ρ	m_{K^*}	m_ϕ	f_ρ	f_{K^*}	f_ϕ
Calc. [24]	138	497	93	109	742	936	1072	207	241	259
Expt. [25]	138	496	92	113	771	892	1019	217	227	228
Rel. Error					0.04	-0.05	-0.05	0.05	-0.06	-0.14

description of hadrons requires $\sigma^\Delta \sim 25 \text{ GeV/fm}$ [6] and that is obtained with [24]

$$D = (0.96 \text{ GeV})^2. \quad (57)$$

This value of the model’s infrared mass-scale parameter and the two current-quark masses

$$m_u(1 \text{ GeV}) = 5.5 \text{ MeV}, \quad m_s(1 \text{ GeV}) = 125 \text{ MeV}, \quad (58)$$

defined using the one-loop expression

$$\frac{m(\zeta)}{m(\zeta')} = Z_m(\zeta', \zeta) \stackrel{1\text{-loop}}{=} \left(\frac{\ln[\zeta'/\Lambda_{\text{QCD}}]}{\ln[\zeta/\Lambda_{\text{QCD}}]} \right)^{\gamma_m} \quad (59)$$

to evolve $m_u(19 \text{ GeV}) = 3.7 \text{ MeV}$ and $m_s(19 \text{ GeV}) = 85 \text{ MeV}$, were obtained in Ref. [24] by requiring a least-squares fit to the π - and K -meson observables listed in Table 2. The procedure was straightforward: the rainbow gap equation [Eqs. (7), (15), (55)] was solved with a given parameter set and the output used to complete the kernels in the homogeneous ladder BSEs for the π - and K -mesons [Eqs. (14), (15), (37), (38) with τ^j for the π channel and $\tau^j \rightarrow T^{K^+} = \frac{1}{2}(\lambda^4 + i\lambda^5)$ for the K]. These BSEs were solved to obtain the π - and K -meson masses, and the Bethe-Salpeter amplitudes. Combining this information delivers the leptonic decay constants via Eq. (53). This was repeated as necessary to arrive at the results in Table 2. The model gives a vacuum quark condensate

$$-\langle \bar{q}q \rangle_{1 \text{ GeV}}^0 = (0.242 \text{ GeV})^3, \quad (60)$$

calculated from Eq. (50) and evolved using the one-loop expression in Eq. (59).

With the model’s single parameter fixed, and the dressed-quark propagator determined, it is straightforward to compose and solve the homogeneous BSE for vector mesons. This yields predictions, also listed in Table 2, for the vector

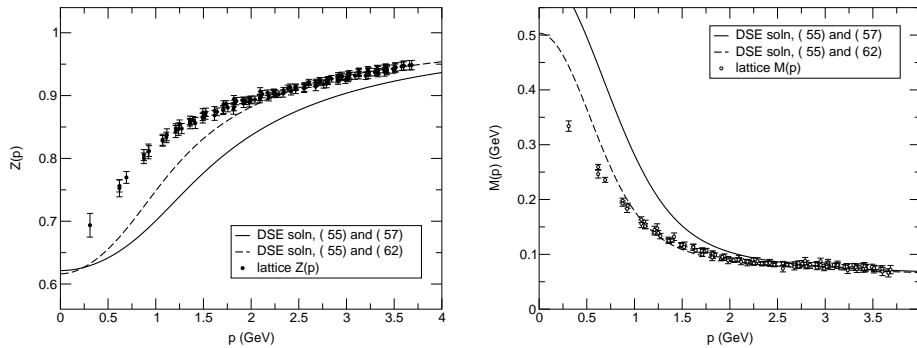


Fig. 5. Left panel – wave function renormalisation: solution of the gap equation using Eqs. (55), (57) (*solid curve*); solution using Eqs. (55), (62) (*dashed-curve*); quenched lattice-QCD simulations [26], obtained with $m = 0.036/a \sim 60$ MeV (*data*). The DSE study used a renormalisation point $\zeta = 19$ GeV and a current-quark mass $0.6 m_s^{1 \text{ GeV}}$ [Eq. (58)], to enable a direct comparison with the lattice data. Right panel – mass function. (Adapted from Ref. [7].)

meson masses and electroweak decay constants [11]

$$f_H^V M_H^V = \frac{1}{3} Z_2 \text{tr} \int_q^A (T^H)^T \gamma_\mu \mathcal{S}(q_+) \Gamma_\mu^H(q; P) \mathcal{S}(q_-), \quad (61)$$

where M_H^V is the meson’s mass and $P_\mu \Gamma_\mu^H(q; P) = 0$ for $P^2 = -(M_H^V)^2$; i.e., the Bethe-Salpeter amplitude is transverse. f_H^V characterises decays such as $\rho \rightarrow e^+ e^-$, $\tau \rightarrow K^* \nu_\tau$.

Given the discussion in Sec. 2, the phenomenological success of the rainbow-ladder kernel, manifest in the results of Table 2, is unsurprising and, indeed, was to be expected.

3.2 Comparison with Lattice Simulations

The solution of the gap equation has long been of interest in grappling with DCSB in QCD and hence, in Figs. 5, I depict the scalar functions characterising the renormalised dressed-quark propagator: the wave function renormalisation, $Z(p^2)$, and mass function, $M(p^2)$, obtained by solving Eq. (15) using Eq. (55). The infrared suppression of $Z(p^2)$ and enhancement of $M(p^2)$ are longstanding predictions of DSE studies [1]. Indeed, this property of asymptotically free theories was elucidated in Refs. [16] and could be anticipated from studies of strong coupling QED [27]. The prediction has recently been confirmed in numerical simulations of quenched lattice-QCD, as is evident in the figures.

It is not yet possible to reliably determine the behaviour of lattice Schwinger functions for current-quark masses that are a realistic approximation to those of the u - and d -quarks. A veracious lattice estimate of m_π , f_π , $\langle \bar{q}q \rangle^0$ is therefore absent. To obtain such an estimate, Ref. [7] used the rainbow kernel described

herein and varied (D, ω) in order to reproduce the quenched lattice-QCD data. A best fit was obtained with

$$D = (0.74 \text{ GeV})^2, \quad \omega = 0.3 \text{ GeV}, \quad (62)$$

at a current-quark mass of $0.6 m_s^{1 \text{ GeV}} \approx 14 m_u$ [Eq. (58)] chosen to coincide with that employed in the lattice simulation. Constructing and solving the homogeneous BSE for a pion-like bound state composed of quarks with this current-mass yields

$$m_\pi^{m_q \sim 14 m_u} = 0.48 \text{ GeV}, \quad f_\pi^{m_q \sim 14 m_u} = 0.094 \text{ GeV}. \quad (63)$$

The parameters in Eq. (62) give chiral limit results [7]:

$$f_\pi^0 = 0.068 \text{ GeV}, \quad -\langle \bar{q}q \rangle_{1 \text{ GeV}}^0 = (0.19 \text{ GeV})^3, \quad (64)$$

whereas Eqs. (56), (57) give $f_\pi^0 = 0.088 \text{ GeV}$. These results have been confirmed in a more detailed analysis [28] and this correspondence suggests that chiral and physical pion observables are materially underestimated in the quenched theory: $|\langle \bar{q}q \rangle|$ by a factor of two and f_π by 30%.

The rainbow-ladder kernel has also been employed in an analysis of a trajectory of fictitious pseudoscalar mesons, all composed of equally massive constituents [29] (The only physical state on this trajectory is the pion.) The DSE study predicts [30]

$$\frac{m_{H_{m=2m_s}}}{m_{H_{m=m_s}}} = 2.2, \quad (65)$$

in agreement with a result of recent quenched lattice simulations [31]. The DSE study provides an intuitive understanding of this result, showing that it owes itself to a large value of the in-hadron condensates for light-quark mesons; e.g., $\langle \bar{q}q \rangle_{1 \text{ GeV}}^{s\bar{s}} = (-0.32 \text{ GeV})^3$ [6], and thereby confirms the large-magnitude condensate version of chiral perturbation theory, an observation also supported by Eq. (64). References [29,32] also provide vector meson trajectories.

3.3 *Ab Initio* Calculation of Meson Properties

The renormalisation-group-improved rainbow-ladder kernel defined with Eq. (55) has been employed to predict a wide range of meson observables, and this is reviewed in Ref. [4]. These results; e.g., those for vector mesons in Table 2, are true predictions, in the sense that the model's mass-scale was fixed, as described in connection with Eq. (57), and every element in each calculation was completely determined by, and calculated from, that kernel.

A particular success was the calculation of the electromagnetic pion form factor, which is described in Refs. [33,34]. The result is depicted in Fig. 6, wherein it is compared with the most recent experimental data [37]. It is noteworthy that all other pre-existing calculations are uniformly two – four standard deviations below that $Q^2 F_\pi(Q^2)$ data.⁶

⁶ The nature and meaning of vector dominance is discussed in Sec. 2.3.1 of Ref. [39], Sec. 2.3 of Ref. [2] and Sec. 4.3 of Ref. [4]: the low- q^2 behaviour of the pion form factor

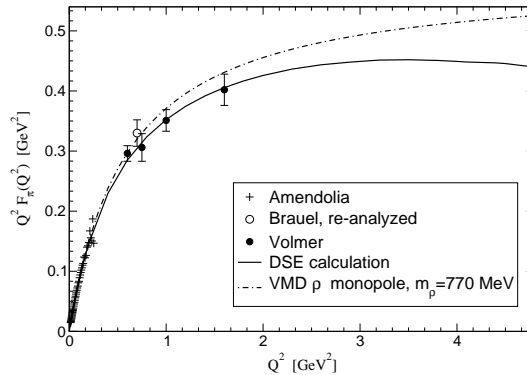


Fig. 6. Impulse approximation DSE prediction for $q^2 F_\pi(q^2)$ obtained in a parameter-free application of the renormalisation-group-improved rainbow-ladder truncation, Eqs. (55), (57). The data are from Refs. [35,36,37]. (Adapted from Ref. [38].)

In this connection one should also note that it is a model independent DSE prediction [40] that electromagnetic elastic meson form factors display

$$q^2 F(q^2) = \text{constant}, \quad q^2 \gg \Lambda_{\text{QCD}}^2, \quad (66)$$

with calculable $(\ln q^2/\Lambda_{\text{QCD}}^2)^d$ corrections, where d is an anomalous dimension. This agrees with earlier perturbative QCD analyses [41,42]. However, to obtain this result in covariant gauges it is crucial to retain the pseudovector components of the Bethe-Salpeter amplitude in Eq. (38): F_π , G_π . (NB. The quark-level Goldberger-Treiman relations, Eqs. (42), prove them to be nonzero.) Without these amplitudes [39], $q^2 F(q^2) \propto 1/q^2$. The calculation of Ref. [40] suggests that the perturbative behaviour of Eq. (66) is unambiguously evident for $q^2 \gtrsim 15 \text{ GeV}^2$. Owing to challenges in the numerical analysis, the *ab initio* calculations of Ref. [34] cannot yet make a prediction for the onset of the perturbative domain but progress in remedying that is being made [43].

Another very instructive success is the study of π - π scattering, wherein a range of new challenges arise whose quiddity and natural resolution via a symmetry-preserving truncation of the DSEs is explained in Sec. 4.6 of Ref. [4], which reviews the seminal work of Refs. [44]. It is worth remarking, too, that with a systematic and nonperturbative DSE truncation scheme, all consequences of the Abelian anomaly and Wess-Zumino term are obtained exactly, without fine tuning [39,40,45,46,47,48].

3.4 Heavier Mesons

The meson spectrum contains [25] four little-studied axial-vector mesons composed of u - and d -quarks. They appear as isospin $I = 0, 1$ partners (in the isospin is necessarily dominated by the lowest mass resonance in the $J^{PC} = 1^{--}$ channel. Any realistic calculation will predict that and also a deviation from dominance by the ρ -meson pole alone as spacelike- q^2 increases.

manner of the ω and ρ): $h_1(1170)$, $b_1(1235)$; and $f_1(1285)$, $a_1(1260)$, and differ in their charge-parity: $J^{PC} = 1^{+-}$ for h_1 , b_1 ; and $J^{PC} = 1^{++}$ for f_1 , a_1 . In the $q\bar{q}$ constituent quark model the b_1 is represented as a constituent-quark and -antiquark with total spin $S = 0$ and angular momentum $L = 1$, while in the a_1 the quark and antiquark have $S = 1$ and $L = 1$. It is therefore apparent that in this model the b_1 is an orbital excitation of the π , and the a_1 is an orbital excitation and axial-vector partner of the ρ . In QCD the J^{PC} characteristics of a quark-antiquark bound state are manifest in the structure of its Bethe-Salpeter amplitude [13]. This amplitude is a valuable intuitive guide and, in cases where a $q\bar{q}$ constituent quark model analogue exists, it incorporates and extends the information present in that analogue's quantum mechanical wave function.

Three of the axial-vector mesons decay predominantly into two-body final states containing a vector meson and a pion: $h_1 \rightarrow \rho\pi$; $b_1 \rightarrow \omega\pi$; $a_1 \rightarrow \rho\pi$. With a $J = 1$ meson in both the initial and final state these three decays proceed via two partial waves (S , D), and therefore probe aspects of hadron structure inaccessible in simpler processes involving only spinless mesons in the final state, such as $\rho \rightarrow \pi\pi$. For example and of importance, in constituent-quark-like models the D/S amplitude ratio is very sensitive [49] to the nature of the phenomenological long-range confining interaction.

The additional insight and model constraints that such processes can provide is particularly important now as a systematic search and classification of “exotic” states in the light meson sector becomes feasible experimentally. I note that a meson is labelled “exotic” if it is characterised by a value of J^{PC} which is unobtainable in the $q\bar{q}$ constituent quark model; e.g., the experimentally observed [50] $\pi_1(1600)$, a 1.6 GeV $J^{PC} = 1^{-+}$ state. Such unusual charge parity states are a necessary feature of a field theoretical description of quark-antiquark bound states [13] with BSE studies typically yielding [51] masses approximately twice as large as that of the natural charge parity partner and, in particular, a $J^{PC} = 1^{-+}$ meson with a mass ~ 1.5 GeV [52].

In appreciation of these points, Ref. [53] used the simple DSE-based model of Ref. [51] in a simultaneous study of axial-vector meson decays, $\rho \rightarrow \pi\pi$ decay, and the electroweak decay constants of the mesons involved. The results are instructive. It was found that the rainbow-ladder truncation is capable of simultaneously providing a good description of these observables but that the D/S partial-wave ratio in the decays of axial-vector mesons is indeed very sensitive to details of the long-range part of a model interaction; i.e., to the expression of light-quark confinement. This is perhaps unsurprising given that the mass of each axial-vector meson mass is significantly greater than $2M(0)$; namely, twice the constituent-quark mass-scale. Unfortunately, more sophisticated calculations are lacking. This collection of experimentally well-understood mesons has many lessons to teach and should no longer be ignored.

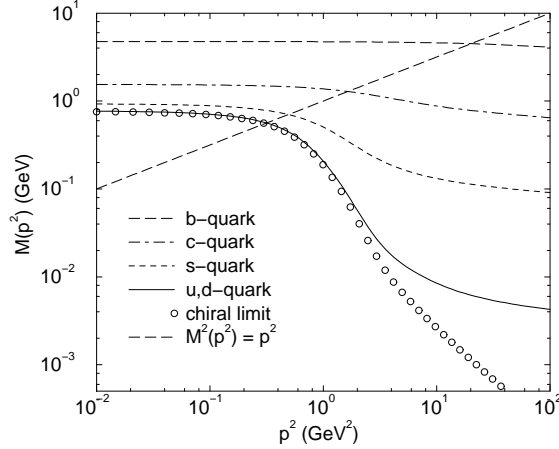


Fig. 7. Quark mass function obtained as a solution of Eq. (67) using the rainbow truncation, discussed in connection with Eqs. (12) – (15), and the interaction of Eq. (55) with current-quark masses, fixed at $\zeta = 19$ GeV: $m_{u,d}(\zeta) = 3.7$ MeV, $m_s(\zeta) = 82$ MeV, $m_c(\zeta) = 0.58$ GeV and $m_b(\zeta) = 3.8$ GeV. The indicated solutions of $M^2(p^2) = p^2$ define a Euclidean constituent-quark mass, M_f^E , which takes the values: $M_u^E = 0.56$ GeV, $M_s^E = 0.70$ GeV, $M_c^E = 1.3$ GeV, $M_b^E = 4.6$ GeV.

4 Heavy Quarks

4.1 Features of the Mass Function

The DSE methods described hitherto have been applied to mesons involving heavy-quarks [11,54,55] and in this case there is a natural simplification. To begin, one focuses on the fact that mesons, whether heavy or light, are bound states of a dressed-quark and -antiquark, with the dressing described by the gap equation, Eq. (1), written explicitly again here with the addition of flavour label, $f (= u, d, s, c, b)$:

$$S_f(p)^{-1} = i\gamma \cdot p A_f(p^2) + B_f(p^2) = A_f(p^2) [i\gamma \cdot p + M_f(p^2)] \quad (67)$$

$$= Z_2(i\gamma \cdot p + m_f^{\text{bm}}) + Z_1 \int_q^A g^2 D_{\mu\nu}(p-q) \frac{\lambda^a}{2} \gamma_\mu S_f(q) \Gamma_\nu^{fa}(q,p). \quad (68)$$

The other elements of Eq. (68) will already be familiar.

The qualitative features of the gap equation's solution are known and typical mass functions, $M_f(p^2)$, are depicted in Fig. 7. There is some quantitative model-dependence in the momentum-evolution of the mass-function into the infrared. However, with any *Ansatz* for the effective interaction that provides an accurate description of $f_{\pi,K}$ and $m_{\pi,K}$, one obtains solutions with profiles like those illustrated in the figure. Owing to Eq. (13) the ultraviolet behaviour is naturally fixed, namely, it is given by Eq. (5) for massive quarks and by Eq. (43) in the chiral limit.

It is apparent in the figure that as p^2 decreases the chiral-limit and u, d -quark mass functions evolve to coincidence. This feature signals a transition from the perturbative to the nonperturbative domain. Furthermore, since the chiral limit mass-function is nonzero *only* because of the nonperturbative DCSB mechanism, whereas the u, d -quark mass function is purely perturbative at $p^2 > 20 \text{ GeV}^2$, it also indicates clearly that the DCSB mechanism has a significant impact on the propagation characteristics of u, d, s -quarks. However, it is conspicuous in Fig. 7 that this is not the case for the b -quark. Its large current-quark mass almost entirely suppresses momentum-dependent dressing so that $M_b(p^2)$ is nearly constant on a substantial domain. The same is true to a lesser extent for the c -quark.

The quantity $\mathcal{L}_f := M_f^E/m_f(\zeta)$ provides a single quantitative measure of the importance of the DCSB mechanism; i.e., nonperturbative effects, in modifying the propagation characteristics of a given quark flavour. In this particular illustration it takes the values

$$\frac{f}{\mathcal{L}_f} \left| \begin{array}{c|ccc} u, d & s & c & b \\ \hline 150 & 10 & 2.2 & 1.2 \end{array} \right., \quad (69)$$

which are representative: for light-quarks $\mathcal{L}_{q=u,d,s} \sim 10$ -100; while for heavy-quarks $\mathcal{L}_{Q=c,b} \sim 1$. They also highlight the existence of a mass-scale, M_χ , characteristic of DCSB: the propagation characteristics of a flavour with $m_f(\zeta) \leq M_\chi$ are significantly altered by the DCSB mechanism, while momentum-dependent dressing is almost irrelevant for flavours with $m_f(\zeta) \gg M_\chi$. It is evident and unsurprising that $M_\chi \sim 0.2 \text{ GeV} \sim \Lambda_{\text{QCD}}$. Consequently one anticipates that the propagation of c, b -quarks should be described well by replacing their mass-functions with a constant; viz., writing [11]

$$S_Q(p) = \frac{1}{i\gamma \cdot p + \hat{M}_Q}, \quad Q = c, b, \quad (70)$$

where \hat{M}_Q is a constituent-heavy-quark mass parameter.⁷

When considering a meson with an heavy-quark constituent one can proceed further, as in heavy-quark effective theory (HQET) [56], allow the heaviest quark to carry all the heavy-meson's momentum: $P_\mu =: m_H v_\mu =: (\hat{M}_Q + E_H)v_\mu$, and write

$$S_Q(k + P) = \frac{1}{2} \frac{1 - i\gamma \cdot v}{k \cdot v - E_H} + \text{O} \left(\frac{|k|}{\hat{M}_Q}, \frac{E_H}{\hat{M}_Q} \right), \quad (71)$$

where k is the momentum of the lighter constituent. It is apparent from the study of light-meson properties that in the calculation of observables the meson's Bethe-Salpeter amplitude will limit the range of $|k|$ so that Eq. (71) will only be a good approximation if *both* the momentum-space width of the amplitude, ω_H , and the binding energy, E_H , are significantly less than \hat{M}_Q .

In Ref. [55] the propagation of c - and b -quarks was described by Eq. (71), with a goal of exploring the fidelity of this idealisation, and it was found to allow

⁷ Although not illustrated explicitly, when $M_f(p^2) \approx \text{const.}$, $A_f(p^2) \approx 1$ in Eq. (67).

for a uniformly good description of B_f -meson leptonic and semileptonic decays with heavy- and light-pseudoscalar final states. In that study, $\omega_{B_f} \approx 1.3$ GeV and $E_{B_f} \approx 0.70$ GeV, both of which are small compared with $\hat{M}_b \approx 4.6$ GeV in Fig. 7. Hence the accuracy of the approximation could be foreseen. It is reasonable to suppose that $\omega_D \approx \omega_B$ and $E_D \approx E_B$, since they must be identical in the limit of exact heavy-quark symmetry. Thus in processes involving the weak decay of a c -quark ($\hat{M}_c \approx 1.3$ GeV) where a D_f -meson is the heaviest participant, Eq. (71) must be inadequate; an expectation verified in Ref. [55].

The failure of Eq. (71) for the c -quark complicates or precludes the development of a common understanding of D_f - and B_f -meson observables using such contemporary theoretical tools as HQET and light cone sum rules. However, as shown in Ref. [11] and I will illustrate, the constituent-like dressed-heavy-quark propagator of Eq. (70) can still be used to effect a unified, accurate simplification in the study of these observables.

4.2 Leptonic Decays

Pseudoscalar Mesons. The leptonic decay of a pseudoscalar meson, $P(p)$, is described by the matrix element (Sec. 2.4)

$$f_P p_\mu := \langle 0 | \bar{\mathcal{Q}} (T^P)^T \gamma_\mu \gamma_5 \mathcal{Q} | P(p) \rangle = \text{tr} Z_2 \int_k^A (T^P)^T \gamma_5 \gamma_\mu \chi_P(k; p), \quad (72)$$

where $\mathcal{Q} = \text{column}(u, d, s, c, b)$ and here I have adopted a charged particle normalisation, which yields results for f_P a factor of $\sqrt{2}$ larger than Eq. (53) and is conventional in studying heavy-quark systems.

In Eq. (72), χ_P is the meson's Bethe-Salpeter wave function, related to its amplitude, Γ_P , via Eq. (31) and normalised canonically as described in connection with Eq. (30). Using Eq. (71), it follows from the canonical normalisation condition that

$$\mathcal{G}_P(k; p) := \frac{1}{\sqrt{m_P}} \Gamma_P(k; p) < \infty, \quad m_P \rightarrow \infty; \quad (73)$$

i.e., $\mathcal{G}_P(k; p)$ so-defined is mass-independent in the heavy-quark limit. Using this result plus Eq. (71) one finds from Eq. (72) [54]

$$f_P \propto \frac{1}{\sqrt{m_P}}, \quad m_P \rightarrow \infty. \quad (74)$$

Equation (74) is a model-independent result and a well-known general consequence of heavy-quark symmetry [56]. However, the value of the hadron mass at which this behaviour becomes evident is unknown. It is clear from Table 2 that, experimentally,

$$f_\pi = 131 \text{ MeV} < f_K = 160 \text{ MeV}. \quad (75)$$

Furthermore, direct DSE studies following the method described in Sec. 3.3 show that for pseudoscalar mesons $u\bar{f}$, composed of a single u, d -quark and an anti-quark of mass m_f , $f_P(m_P)$ is a monotonically increasing concave-down function on $m_P \in [0, 0.9]$ GeV, where m_P is the calculated mass of this composite system, and likely on a larger domain [32]. On the other hand, numerical simulations of quenched lattice-QCD indicate [57]

$$f_D = 200 \pm 30 \text{ MeV} > f_B = 170 \pm 35 \text{ MeV}. \quad (76)$$

In simulations of lattice-QCD with two flavours of sea quarks both of these decay constants increase in magnitude but there is no sign that the ordering is reversed [57,58]. The information in Eqs. (75), (76) is depicted in Fig. 8. This and analysis to be reviewed subsequently suggest that D-mesons lie outside the domain on which Eq. (74) is a reliable tool.

Vector Mesons. The leptonic decay constant, f_V , for a vector meson with mass M_V is given in Eq. (61) and adapting the analysis that leads to Eq. (74) one finds readily

$$f_V \propto \frac{1}{\sqrt{M_V}}, \quad M_V \rightarrow \infty, \quad (77)$$

which again is a model-independent result. Moreover, since the pseudoscalar and vector meson Bethe-Salpeter amplitudes become identical in the heavy-quark limit, it follows that [11]

$$f_V = f_P, \quad M_V = m_P, \quad \text{in the limit } m_P \rightarrow \infty. \quad (78)$$

4.3 Heavy-Meson Masses

More can be learnt from the pseudoscalar meson mass formula in Eq. (52). Using Eq. (74), and applying to Eq. (54) the analysis from which it follows, one obtains

$$-\langle \bar{q}q \rangle_\zeta^P = \text{constant}, \quad \text{as } m_P \rightarrow \infty \quad (79)$$

and consequently [10,11]

$$m_P \propto \hat{m}_Q, \quad \hat{m}_Q \rightarrow \infty, \quad (80)$$

where \hat{m}_Q is the renormalisation-group-invariant current-quark mass of the flavour-nonsinglet pseudoscalar meson's heaviest constituent. This is the result one would have guessed from constituent-quark models but here I have outlined a direct proof in QCD.

Equation (47) is thus seen to be a single formula that unifies the masses of light- and heavy-quark mesons. This aspect has been quantitatively explored using the rainbow-ladder kernel described in Sec. 3, with the results illustrated in Fig. 9. Therein the calculated mass of a $u\bar{f}$ pseudoscalar meson is plotted

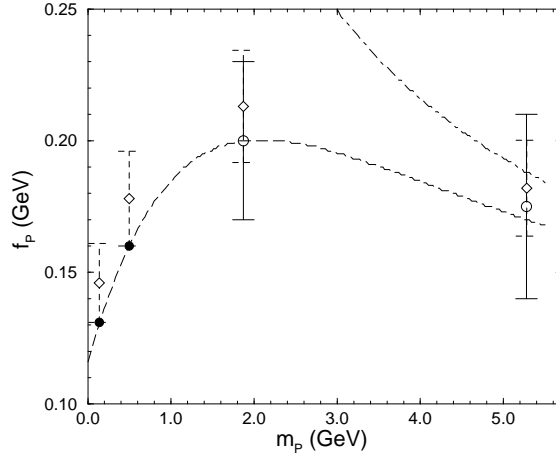


Fig. 8. Experimental values of $f_{\pi, K}$ (Eq. (75), *filled circles*); lattice estimates of $f_{D, B}$ (Eq. (76), *open circles*); values of $f_{\pi, K, D, B}$ calculated in Ref. [11] (*open diamonds*). Least-squares fit to the experimental values and lattice estimates (*dashed curve*): $f_P^2 = (0.013 + 0.028 m_P)/(1 + 0.055 m_P + 0.15 m_P^2)$, which exhibits the large- m_P limit of Eq. (74); the large- m_P limit of this fit (*dot-dashed curve*). (Adapted from Ref. [11].)

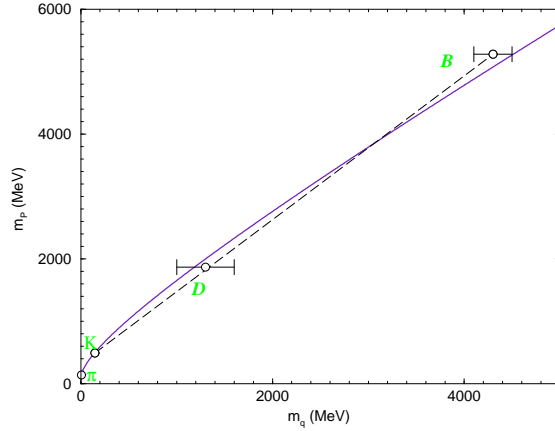


Fig. 9. Pseudoscalar $u\bar{q}$ meson's mass as a function of $m_q(\zeta)$, $\zeta = 19$ GeV, with a fixed value of $m_u(\zeta)$ corresponding to $m_u(1 \text{ GeV}) = 5.5$ MeV, Eq. (58) (*solid line*). The experimental data points are from Ref. [25] as are the errors assigned to the associated heavy-quark masses. A straight line is drawn through the K, D, B masses (*dashed curve*). (Adapted from Ref. [59]. See also Ref. [32].)

as a function of $m_f(\zeta)$, with $m_u(\zeta)$ fixed at the value in Eq. (58). The DSE calculations are depicted by the solid curve, which is [29] (in MeV)

$$m_P = 83 + 500\sqrt{\mathcal{X}} + 310 \mathcal{X}, \quad \mathcal{X} = m_q^\zeta / \Lambda_{\text{QCD}}. \quad (81)$$

The curvature appears slight in the figure but that is misleading: the nonlinear term in Eq. (81) accounts for almost all of m_π (the Gell-Mann–Oakes–Renner relation is nearly exact for the pion) and 80% of m_K . NB. The dashed line in Fig. 9 fits the K , D , B subset of the data exactly. It is drawn to illustrate how easily one can be misled. Without careful calculation one might infer from this apparent agreement that the large- m_q limit of Eq. (47) is already manifest at the s -quark mass whereas, in reality, the linear term only becomes dominant for $m_q \gtrsim 1$ GeV, providing 50% of m_D and 67% of m_B . The model predicts, via Eq. (59), $m_c^{1\text{GeV}} = 1.1$ GeV and $m_b^{1\text{GeV}} = 4.2$ GeV, values that are typical of Poincaré covariant treatments.

4.4 Semileptonic Transition Form Factors

Pseudoscalar meson in the final state. The transition: $P_1(p_1) \rightarrow P_2(p_2) \ell \nu$, where P_1 represents either a B - or D -meson and P_2 can be a D , K or π , is described by the invariant amplitude

$$A(P_1 \rightarrow P_2 \ell \nu) = \frac{G_F}{\sqrt{2}} V_{f'f} \bar{\ell} \gamma_\mu (1 - \gamma_5) \nu M_\mu^{P_1 P_2}(p_1, p_2), \quad (82)$$

where $G_F = 1.166 \times 10^{-5} \text{ GeV}^{-2}$, $V_{f'f}$ is the relevant element of the Cabibbo-Kobayashi-Maskawa (CKM) matrix, and the hadronic current is

$$M_\mu^{P_1 P_2}(p_1, p_2) := \langle P_2(p_2) | \bar{f}' \gamma_\mu f | P_1(p_1) \rangle = f_+(t) (p_1 + p_2)_\mu + f_-(t) q_\mu, \quad (83)$$

with $t := -q^2 = -(p_1 - p_2)^2$. The transition form factors, $f_\pm(t)$, contain all the information about strong-interaction effects in these processes, and their accurate calculation is essential for a reliable determination of the CKM matrix elements from a measurement of the decay width ($t_\pm := (m_{P_1} \pm m_{P_2})^2$):

$$\Gamma(P_1 \rightarrow P_2 \ell \nu) = \frac{G_F^2}{192\pi^3} |V_{f'f}|^2 \frac{1}{m_{P_1}^3} \int_0^{t_-} dt |f_+(t)|^2 [(t_+ - t)(t_- - t)]^{3/2}. \quad (84)$$

The related study of light-meson initial states is described in Refs. [60].

Vector meson in the final state. The transition: $P(p_1) \rightarrow V_\lambda(p_2) \ell \nu$, with P either a B or D and V_λ a D^* , K^* or ρ , is described by the invariant amplitude

$$A(P \rightarrow V_\lambda \ell \nu) = \frac{G_F}{\sqrt{2}} V_{f'f} \bar{\ell} i \gamma_\mu (1 - \gamma_5) \nu \epsilon_\nu^\lambda(p_2) M_{\mu\nu}^{PV_\lambda}(p_1, p_2), \quad (85)$$

in which the hadronic tensor involves four scalar functions

$$\begin{aligned} \epsilon_\nu^\lambda(p_2) M_{\mu\nu}^{PV_\lambda}(p_1, p_2) &= \epsilon_\mu^\lambda (m_P + M_V) A_1(t) + (p_1 + p_2)_\mu \epsilon^\lambda \cdot q \frac{A_2(t)}{m_P + M_V} \\ &+ q_\mu \epsilon^\lambda \cdot q \frac{A_3(t)}{m_P + M_V} + \varepsilon_{\mu\nu\alpha\beta} \epsilon_\nu^\lambda p_{1\alpha} p_{2\beta} \frac{2V(t)}{m_P + M_V}. \end{aligned} \quad (86)$$

Introducing three helicity amplitudes

$$H_{\pm} = (m_P + M_V) A_1(t) \mp \frac{\lambda^{\frac{1}{2}}(m_P^2, M_V^2, t)}{m_P + M_V} V(t), \quad (87)$$

$$H_0 = \frac{1}{2M_V\sqrt{t}} \left([m_P^2 - M_V^2 - t] [m_P + M_V] A_1(t) - \frac{\lambda(m_P^2, M_V^2, t)}{m_P + M_V} A_2(t) \right), \quad (88)$$

where $\lambda(m_P^2, M_V^2, t) = [t_+ - t][t_- - t]$, $t_{\pm} = (m_P \pm M_V)^2$, the transition rates

$$\frac{d\Gamma_{\pm,0}}{dt} = \frac{G_F^2}{192\pi^3 m_{P_1}^3} |V_{f'f}|^2 t \lambda^{\frac{1}{2}}(m_P^2, M_V^2, t) |H_{\pm,0}(t)|^2, \quad (89)$$

from which one obtains the transverse and longitudinal rates

$$\frac{d\Gamma_T}{dt} = \frac{d\Gamma_+}{dt} + \frac{d\Gamma_-}{dt}, \quad \Gamma_T = \int_0^{t_-} dt \frac{d\Gamma_T}{dt}, \quad (90)$$

$$\frac{d\Gamma_L}{dt} = \frac{d\Gamma_0}{dt}, \quad \Gamma_L = \int_0^{t_-} dt \frac{d\Gamma_L}{dt}, \quad (91)$$

wherefrom the total width $\Gamma = \Gamma_T + \Gamma_L$. The polarisation ratio and forward-backward asymmetry are

$$\alpha = 2 \frac{\Gamma_L}{\Gamma_T} - 1, \quad A_{\text{FB}} = \frac{3}{4} \frac{\Gamma_- - \Gamma_+}{\Gamma}. \quad (92)$$

4.5 Impulse Approximation

As explained and illustrated in Ref. [4], the impulse approximation is accurate for three point functions and applied to these transition form factors it yields

$$\begin{aligned} \mathcal{H}_{\mu}^{PX}(p_1, p_2) = \\ 2N_c \text{tr}_D \int_k^{\Lambda} \bar{\Gamma}_X(k; -p_2) S_q(k_2) i\mathcal{O}_{\mu}^{qQ}(k_2, k_1) S_Q(k_1) \Gamma_P(k; p_1) S_{q'}(k), \end{aligned} \quad (93)$$

wherein the flavour structure is made explicit, $k_{1,2} = k + p_{1,2}$ and:

$$\mathcal{H}_{\mu}^{P_1 X = P_2}(p_1, p_2) = M_{\mu}^{P_1 P_2}(p_1, p_2), \quad (94)$$

$$\mathcal{H}_{\mu}^{P X = V^{\lambda}}(p_1, p_2) = \epsilon_{\nu}^{\lambda}(p_2) M_{\mu\nu}^{P V^{\lambda}}(p_1, p_2); \quad (95)$$

$\Gamma_{X=V^{\lambda}}(k; p) = \epsilon^{\lambda}(p) \cdot \Gamma^V(k; p)$; and $\mathcal{O}_{\mu}^{qQ}(k_2, k_1)$ is the dressed-quark-W-boson vertex, which in weak decays of heavy-quarks is well approximated by [54,55]

$$\mathcal{O}_{\mu}^{qQ}(k_2, k_1) = \gamma_{\mu} (1 - \gamma_5) \quad (96)$$

because $A_Q(p^2) \approx \text{const.}$ and $M_Q(p^2) \approx \text{const.}$ for heavy-quarks (recall Fig. 7.)

Quark Propagators. It is plain that to evaluate $\mathcal{H}_\mu^{P_1 X}(p_1, p_2)$ a specific form for the dressed-quark propagators is required. Equation (70) provides a good approximation for the heavier quarks, $Q = c, b$, as explained in Sec. 4.1, and this was used in Ref. [11] with \hat{M}_Q treated as free parameters.

For the light-quark propagators:

$$S_f(p) = -i\gamma \cdot p \sigma_V^f(p^2) + \sigma_S^f(p^2) = \frac{1}{i\gamma \cdot p A_f(p^2) + B_f(p^2)}, \quad (97)$$

Ref. [11] assumed isospin symmetry and employed the algebraic forms introduced in Ref. [39], which efficiently characterise the essential features of the gap equation's solutions:

$$\bar{\sigma}_S^f(x) = 2\bar{m}_f \mathcal{F}(2(x + \bar{m}_f^2)) + \mathcal{F}(b_1 x) \mathcal{F}(b_3 x) \left[b_0^f + b_2^f \mathcal{F}(\epsilon x) \right], \quad (98)$$

$$\bar{\sigma}_V^f(x) = \frac{2(x + \bar{m}_f^2) - 1 + e^{-2(x + \bar{m}_f^2)}}{2(x + \bar{m}_f^2)^2}, \quad (99)$$

$\mathcal{F}(y) = (1 - e^{-y})/y$, $x = p^2/\lambda^2$; $\bar{m}_f = m_f/\lambda$; and $\bar{\sigma}_S^f(x) = \lambda \sigma_S^f(p^2)$, $\bar{\sigma}_V^f(x) = \lambda^2 \sigma_V^f(p^2)$, with λ a mass scale. The parameters are the current-quark mass, \bar{m} , and $b_{0,1,2,3}$, about which I shall subsequently explain more.

This algebraic form combines the effects of confinement⁸ and DCSB with free-particle behaviour at large, spacelike p^2 . One characteristic of DCSB is the appearance of a nonzero vacuum quark condensate and using this parametrisation in Eq. (50) yields

$$-\langle \bar{u}u \rangle_\zeta = \lambda^3 \frac{3}{4\pi^2} \frac{b_0^u}{b_1^u b_3^u} \ln \frac{\zeta^2}{A_{\text{QCD}}^2}. \quad (100)$$

The simplicity of this result emphasises the utility of an algebraic form for the dressed-quark propagator. That utility is amplified in the calculation of a form factor, which requires the repeated evaluation of a multidimensional integral whose integrand is a complex-valued function, and a functional of the propagator and the Bethe-Salpeter amplitudes.

Bethe-Salpeter Amplitudes. An algebraic parametrisation of the Bethe-Salpeter amplitudes also helps and the quark-level Goldberger-Treiman relation, Eq. (42), suggests a form for light pseudoscalar mesons:

$$\Gamma_P(k; p) = i\gamma_5 \mathcal{E}_P(k^2) = i\gamma_5 \frac{1}{f_P} B_P(k^2), \quad P = \pi, K, \quad (101)$$

⁸ The representation of $S(p)$ as an entire function is motivated by the algebraic solutions of Eq. (1) in Refs. [61]. The concomitant violation of the axiom of *reflection positivity* is a sufficient condition for confinement, as reviewed in Sec. 6.2 of Ref. [1], Sec. 2.2 of Ref. [2] and Sec. 2.4 of Ref. [3].

where $B_P := B_u|_{b_0^u \rightarrow b_0^P}$, obtained from Eq. (97), and $\hat{f}_P = f_P/\sqrt{2}$ because in this Section I use the $f_\pi = 131$ MeV normalisation. $b_0^{\pi,K}$ are two additional parameters. This *Ansatz* omits the pseudovector components of the amplitude but that is not a material defect in applications involving small to intermediate momentum transfers [40]. Equations (52), (54), (101) yield the following expression for the π - and K -meson masses:

$$\hat{f}_P^2 m_P^2 = -(m_u + m_{fP}) \langle \bar{q}q \rangle_{1\text{GeV}^2}^P, \quad (102)$$

where $m_{f\pi} = m_d$, $m_{fK} = m_s$, and

$$- \langle \bar{q}q \rangle_{1\text{GeV}^2}^P = \lambda^3 \ln \frac{1}{\Lambda_{\text{QCD}}^2} \frac{3}{4\pi^2} \frac{b_0^P}{b_1^u b_3^u}, \quad P = \pi, K. \quad (103)$$

In studies of the type reviewed in Sec. 3, this in-hadron condensate takes values $\langle \bar{q}q \rangle_{1\text{GeV}^2}^\pi \approx 1.05 \langle \bar{u}u \rangle_{1\text{GeV}^2}$ and $\langle \bar{q}q \rangle_{1\text{GeV}^2}^K \approx 1.6 \langle \bar{u}u \rangle_{1\text{GeV}^2}$.

Employing algebraic parametrisations of the light vector meson Bethe-Salpeter amplitudes is also a useful expedient and that approach was adopted in Refs. [11,54,55]. Indeed, sophisticated calculations of light vector meson properties based on the rainbow-ladder truncation did not exist at the time of those studies, although it was clear that a given vector meson is narrower in momentum space than its pseudoscalar partner, and that for both vector and pseudoscalar mesons this width increases with the total current-mass of the constituents. These qualitative features were important in the explanation of meson electro-production cross sections [62] and electromagnetic form factors [63], and can be realised in the simple expression

$$\Gamma_\mu^V(k; p) = \frac{1}{\mathcal{N}^V} \left(\gamma_\mu + p_\mu \frac{\gamma \cdot p}{M_V^2} \right) \varphi(k^2), \quad (104)$$

where $\varphi(k^2) = 1/(1+k^4/\omega_V^4)$ with ω_V a parameter and \mathcal{N}^V fixed by the canonical normalisation condition. One expects: $\omega_{K^*} \approx 1.6 \omega_\rho$ [63].

In connection with the impulse approximation to semileptonic transition form factors it remains only to fix the heavy-meson Bethe-Salpeter amplitudes. In this case, too, algebraic parametrisations offer a simple, attractive and expeditious means of proceeding and that again was the approach adopted in Ref. [11]. Therein heavy vector mesons were described by Eq. (104), with $\varphi(k^2) \rightarrow \varphi_H(k^2)$, and heavy pseudoscalar mesons by its analogue:

$$\Gamma_P(k; p) = \frac{1}{\mathcal{N}^P} i \gamma_5 \varphi_H(k^2), \quad (105)$$

where $\varphi_H(k^2) = \exp(-k^2/\omega_H^2)$. The amplitudes are again normalised canonically. Such a parametrisation naturally introduces additional parameters; viz., the widths. The number is kept at two by acknowledging that Bethe-Salpeter amplitudes for truly heavy-mesons must be spin- and flavour-independent and assuming therefore that $\omega_B = \omega_{B^*} = \omega_{B_s}$ and $\omega_D = \omega_{D^*} = \omega_{D_s}$.

4.6 Additional Decay Processes

Many more decays were considered in Ref. [11], with the goal being to determine whether a unified description of light- and heavy-meson observables is possible based simply on the key DSE features of quark dressing and sensible bound state amplitudes. For example, there are experimental constraints on radiative decays $H^* \rightarrow H \gamma$, where $H = D_{(s)}, B_{(s)}$, and so these widths, $\Gamma_{H^* \rightarrow H \gamma}$, were calculated. The strong decays $H^* \rightarrow H \pi$ were also studied. They can be characterised by a coupling constant $g_{H^* H \pi}$, which is calculable even if the process is kinematically forbidden, as is $B^* \rightarrow B \pi$. Lastly, the width for the rare flavour-changing neutral current process $B \rightarrow K^* \gamma$, which proceeds predominantly via the local magnetic penguin operator [64] and can be characterised by a coupling $g_{BK^* \gamma}$, was calculated because data exists and this process might be expected to severely test the framework since it completely exceeds the scope of previous applications.

4.7 Heavy-Quark Symmetry Limits

Equation (71), and Eq. (73) and its natural analogues, can be used to elucidate the heavy-quark symmetry limit of the impulse approximation to any process and many were made explicit in Refs. [11,54,55]. I will only recapitulate on the most straightforward three-point case; namely, the semileptonic heavy \rightarrow heavy transitions. From Eqs. (83), (93) one obtains

$$f_{\pm}(t) = \mathcal{T}_{\pm} \xi_f(w) := \frac{m_{P_2} \pm m_{P_1}}{2\sqrt{m_{P_2} m_{P_1}}} \xi_f(w), \quad (106)$$

$$\xi_f(w) = \kappa_f^2 \frac{N_c}{4\pi^2} \int_0^1 d\tau \frac{1}{W} \int_0^\infty du \varphi_H(z_W)^2 \left[\sigma_S^f(z_W) + \sqrt{\frac{u}{W}} \sigma_V^f(z_W) \right],$$

where: $W = 1 + 2\tau(1 - \tau)(w - 1)$, $z_W = u - 2E_H \sqrt{u/W}$;

$$\frac{1}{m_H} \frac{1}{\kappa_f^2} := \mathcal{N}_P^2 = \mathcal{N}_V^2 = \frac{1}{m_H} \frac{N_c}{4\pi^2} \int_0^\infty du \varphi_H^2(z) \left\{ \sigma_S^f(z) + \sqrt{u} \sigma_V^f(z) \right\}, \quad (107)$$

with $z = u - 2E_H \sqrt{u}$, f labelling the meson's lighter quark and all dimensioned quantities expressed in units of the mass-scale, λ ; and

$$w = \frac{m_{P_1}^2 + m_{P_2}^2 - t}{2m_{P_1} m_{P_2}} = -v_{P_1} \cdot v_{P_2}. \quad (108)$$

The canonical normalisation of the Bethe-Salpeter amplitude automatically ensures

$$\xi_f(w = 1) = 1 \quad (109)$$

and from Eq. (106) follows [54]

$$\rho^2 := - \left. \frac{d\xi_f}{dw} \right|_{w=1} \geq \frac{1}{3}. \quad (110)$$

Semileptonic transitions with heavy vector mesons in the final state, described by Eqs. (86) and (93), can be analysed in the same way, and that yields

$$A_1(t) = \frac{1}{\mathcal{T}_+} \frac{1}{2} (1+w) \xi_f(w), \quad A_2(t) = -A_3(t) = V(t) = \mathcal{T}_+ \xi_f(w). \quad (111)$$

Equations (106), (111) are exemplars of a general result that in the heavy-quark symmetry limit the semileptonic $H_f \rightarrow H'_f$ transitions are described by a single, universal function: $\xi_f(w)$ [65]. In this limit the functions

$$R_1(w) := (1 - t/t_+) \frac{V(t)}{A_1(t)}, \quad R_2(w) := (1 - t/t_+) \frac{A_2(t)}{A_1(t)} \quad (112)$$

are constant (= 1), independent of w .

4.8 Survey of Results for Light- and Heavy-Meson Observables

With every necessary element defined, the calculation of observables is a straightforward numerical exercise. The algebraic *Ansätze* described above involve ten parameters plus four current-quark masses and in Ref. [11] they were fixed via a χ^2 -fit to the $N_{\text{obs}} = 42$ heavy- and light-meson observables in Table 3, a process which yielded [66]

	\bar{m}_f	b_1^f	b_2^f	π	b_0^P	ρ	ω_V^{GeV}	D	ω_H^{GeV}	c	\hat{M}_Q^{GeV}
u	0.00948	2.94	0.733	K	0.204	K^*	0.515	1.81	1.81	1.32	(113)
s	0.210	3.18	0.858	B	0.319	B	0.817	1.81	1.81	4.65	

with $\chi^2/\text{d.o.f} = 1.75$ and $\chi^2/N_{\text{obs}} = 1.17$. The dimensionless u, s current-quark masses correspond to $m_u = 5.4 \text{ MeV}$, $m_s = 119 \text{ MeV}$, and $M_u^E = 0.36 \text{ GeV}$, $M_s^E = 0.49 \text{ GeV}$. Furthermore, $\omega_{K^*}/\omega_\rho = 1.59$, which is identical to the value in Ref. [63].

It is evident that the fitted heavy-quark masses are consistent with the estimates in Ref. [25] and hence that the heavy-meson binding energy is large:

$$E_D := m_D - \hat{M}_c = 0.67 \text{ GeV}, \quad E_B := m_B - \hat{M}_b = 0.70 \text{ GeV}. \quad (114)$$

These values yield $E_D/\hat{M}_c = 0.51$ and $E_B/\hat{M}_b = 0.15$, which furnishes another indication that while an heavy-quark expansion is accurate for the b -quark it will provide a poor approximation for the c -quark. This is emphasised by the value of $\omega_D = \omega_B$, which means that the Compton wavelength of the c -quark is greater than the length-scale characterising the bound state's extent.

With the parameters fixed, in Ref. [11] values for a wide range of other observables were calculated with the vast majority of the results being true predictions. The breadth of application is illustrated in Table 4, and in Fig. 10 which depicts the calculated t -dependence of $B \rightarrow \pi, \rho$ semileptonic transition form factors. I note that now there is a first experimental result for the D^{*+} width [72]: $\Gamma_{D^{*+}} = (96 \pm 4 \pm 22) \text{ keV}$, $g_{D^* D \pi} = 17.9 \pm 0.3 \pm 1.9$. Its confirmation and the gathering of additional information on c -quark mesons is crucial to improving our knowledge of the evolution from the light- to the heavy-quark domain, a transition whose true understanding will significantly enhance our grasp of nonperturbative dynamics.

Table 3. The 16 dimension-GeV (*upper panel*) and 26 dimensionless (*lower panel*) quantities used in the χ^2 -fit of Ref. [11]. The weighting error was the experimental error or 10% of the experimental value, if that is greater, which accounts for a realistic expectation of the model’s accuracy. The light-meson electromagnetic form factors were calculated in impulse approximation [39,40,67] and $\xi(w)$ was obtained from $f_+^{B \rightarrow D}(t)$ via Eq. (106). The values in the “Obs.” column were taken from Refs. [6,25,36,57,68,69,70,71]. (Adapted from Ref. [11].)

	Obs.	Calc.		Obs.	Calc.
f_π	0.131	0.146	m_π	0.138	0.130
f_K	0.160	0.178	m_K	0.496	0.449
$\langle \bar{u}u \rangle^{1/3}$	0.241	0.220	$\langle \bar{s}s \rangle^{1/3}$	0.227	0.199
$\langle \bar{q}q \rangle_\pi^{1/3}$	0.245	0.255	$\langle \bar{q}q \rangle_K^{1/3}$	0.287	0.296
f_ρ	0.216	0.163	f_{K^*}	0.244	0.253
$\Gamma_{\rho\pi\pi}$	0.151	0.118	$\Gamma_{K^*(K\pi)}$	0.051	0.052
f_D	0.200 ± 0.030	0.213	f_{D_s}	0.251 ± 0.030	0.234
f_B	0.170 ± 0.035	0.182	$g_{BK^*\gamma} \hat{M}_b$	2.03 ± 0.62	2.86
$f_+^{B \rightarrow D}(0)$	0.73	0.58	$f_\pi r_\pi$	0.44 ± 0.004	0.44
$F_\pi(3.3 \text{ GeV}^2)$	0.097 ± 0.019	0.077	$B(B \rightarrow D^*)$	0.0453 ± 0.0032	0.052
ρ^2	1.53 ± 0.36	1.84	$\alpha^{B \rightarrow D^*}$	1.25 ± 0.26	0.94
$\xi(1.1)$	0.86 ± 0.03	0.84	$A_{\text{FB}}^{B \rightarrow D^*}$	0.19 ± 0.031	0.24
$\xi(1.2)$	0.75 ± 0.05	0.72	$B(B \rightarrow \pi)$	$(1.8 \pm 0.6) \times 10^{-4}$	2.2
$\xi(1.3)$	0.66 ± 0.06	0.63	$f_+^{B \rightarrow \pi}(14.9 \text{ GeV}^2)$	0.82 ± 0.17	0.82
$\xi(1.4)$	0.59 ± 0.07	0.56	$f_+^{B \rightarrow \pi}(17.9 \text{ GeV}^2)$	1.19 ± 0.28	1.00
$\xi(1.5)$	0.53 ± 0.08	0.50	$f_+^{B \rightarrow \pi}(20.9 \text{ GeV}^2)$	1.89 ± 0.53	1.28
$B(B \rightarrow D)$	0.020 ± 0.007	0.013	$B(B \rightarrow \rho)$	$(2.5 \pm 0.9) \times 10^{-4}$	4.8
$B(D \rightarrow K^*)$	0.047 ± 0.004	0.049	$f_+^{D \rightarrow K}(0)$	0.73	0.61
$\frac{V(0)}{A_1(0)}^{D \rightarrow K^*}$	1.89 ± 0.25	1.74	$f_+^{D \rightarrow \pi}(0)$	0.73	0.67
$\frac{\Gamma_L}{\Gamma_T}^{D \rightarrow K^*}$	1.23 ± 0.13	1.17	$g_{B^* B \pi}$	23.0 ± 5.0	23.2
$\frac{A_2(0)}{A_1(0)}^{D \rightarrow K^*}$	0.73 ± 0.15	0.87	$g_{D^* D \pi}$	10.0 ± 1.3	11.0

Fidelity of heavy-quark symmetry. The universal function characterising semileptonic transitions in the heavy-quark symmetry limit, $\xi(w)$ introduced in Sec. 4.7, can be estimated most reliably from $B \rightarrow D, D^*$ transitions. Using Eq. (106) to infer this function from $f_+^{B \rightarrow D}(t)$, one obtains

$$\xi^{f_+}(1) = 1.08, \quad (115)$$

Table 4. Predictions in Ref. [11] for a selection of observables. The ‘‘Obs.’’ values are extracted from Refs. [25,57,68,72,73]. t_{\max} is the maximum momentum transfer available in the process identified and $\omega_{\max} = \omega(t_{\max})$ calculated from Eq. (108). (Adapted from Ref. [11].)

	Obs.	Calc.		Obs.	Calc.
f_{KrK}	0.472 ± 0.038	0.46	$-f_{K^*}^2 f_{K^0}^2$	$(0.19 \pm 0.05)^2$	$(0.10)^2$
$g_{\rho\pi\pi}$	6.05 ± 0.02	5.27	$\Gamma_{D^{*0}}$ (MeV)	< 2.1	0.020
$g_{K^*K\pi^0}$	6.41 ± 0.06	5.96	$\Gamma_{D^{*+}}$ (keV)	$96 \pm 4 \pm 22$	37.9
g_{ρ}	5.03 ± 0.012	5.27	$\Gamma_{D_s^* D_s \gamma}$ (MeV)	< 1.9	0.001
f_{D^*} (GeV)		0.290	$\Gamma_{B^{*+} B^+ \gamma}$ (keV)		0.030
$f_{D_s^*}$ (GeV)		0.298	$\Gamma_{B^{*0} B^0 \gamma}$ (keV)		0.015
f_{B_s} (GeV)	0.195 ± 0.035	0.194	$\Gamma_{B_s^* B_s \gamma}$ (keV)		0.011
f_{B^*} (GeV)		0.200	$B(D^{*+} \rightarrow D^+ \pi^0)$	0.306 ± 0.025	0.316
$f_{B_s^*}$ (GeV)		0.209	$B(D^{*+} \rightarrow D^0 \pi^+)$	0.683 ± 0.014	0.683
f_{D_s}/f_D	1.10 ± 0.06	1.10	$B(D^{*+} \rightarrow D^+ \gamma)$	$0.011^{+0.021}_{-0.007}$	0.001
f_{B_s}/f_B	1.14 ± 0.08	1.07	$B(D^{*0} \rightarrow D^0 \pi^0)$	0.619 ± 0.029	0.826
f_{D^*}/f_D		1.36	$B(D^{*0} \rightarrow D^0 \gamma)$	0.381 ± 0.029	0.174
f_{B^*}/f_B		1.10	$B(B \rightarrow K^* \gamma)$	$(5.7 \pm 3.3)_{10^{-5}}$	11.4
$R_1^{B \rightarrow D^*}(1)$	1.30 ± 0.39	1.32	$R_2^{B \rightarrow D^*}(1)$	0.64 ± 0.29	1.04
$R_1^{B \rightarrow D^*}(w_{\max})$		1.23	$R_2^{B \rightarrow D^*}(w_{\max})$		0.98
$B(D^+ \rightarrow \rho^0)$		0.032	$\alpha^{D \rightarrow \rho}$		1.03
$B(D^0 \rightarrow K^-)$	0.037 ± 0.002	0.036	$\frac{B(D \rightarrow \rho^0)}{B(D \rightarrow K^*)}$	0.044 ± 0.034	0.065
$A_1^{D \rightarrow K^*}(0)$	0.56 ± 0.04	0.46	$A_1^{D \rightarrow K^*}(t_{\max}^{D \rightarrow K^*})$	0.66 ± 0.05	0.47
$A_2^{D \rightarrow K^*}(0)$	0.39 ± 0.08	0.40	$A_2^{D \rightarrow K^*}(t_{\max}^{D \rightarrow K^*})$	0.46 ± 0.09	0.44
$V^{D \rightarrow K^*}(0)$	1.1 ± 0.2	0.80	$V^{D \rightarrow K^*}(t_{\max}^{D \rightarrow K^*})$	1.4 ± 0.3	0.92
$\frac{B(D^0 \rightarrow \pi)}{B(D^0 \rightarrow K)}$	0.103 ± 0.039	0.098	$f_+^{D \rightarrow K}(t_{\max}^{D \rightarrow K})$	1.31 ± 0.04	1.11
$\frac{f_+^{D \rightarrow \pi}(0)}{f_+^{D \rightarrow K}(0)}$	1.2 ± 0.3	1.10	$f_+^{D \rightarrow \pi}(t_{\max}^{D \rightarrow \pi})$		2.18
$R_1^{D \rightarrow K^*}(1)$		1.72	$R_1^{D \rightarrow K^*}(w_{\max})$		1.74
$R_1^{D \rightarrow \rho}(1)$		2.08	$R_1^{D \rightarrow \rho}(w_{\max})$		2.03

which is a measurable deviation from Eq. (109). The ratio $\xi^{f^+}(w)/\xi^{f^+}(0)$ is depicted in Fig. 11, wherein it is compared with two experimental fits [69]:

$$\xi(w) = 1 - \rho^2 (w - 1), \quad \rho^2 = 0.91 \pm 0.15 \pm 0.16, \quad (116)$$

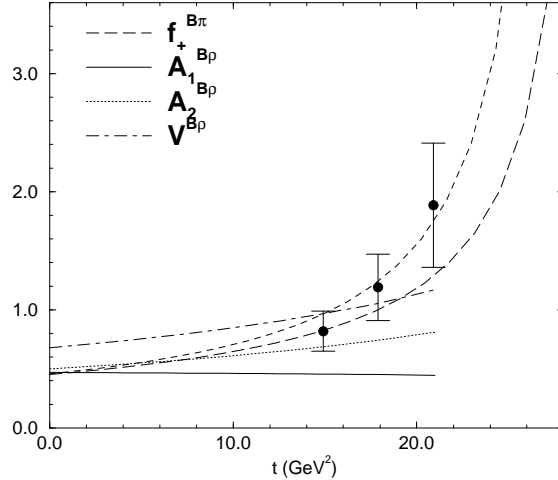


Fig. 10. Semileptonic $B \rightarrow \pi$ and $B \rightarrow \rho$ form factors with, for comparison, data from a lattice simulation [70] and a vector dominance, monopole model: $f_+^{B \rightarrow \pi}(t) = 0.46/(1 - t/m_{B^*}^2)$, $m_{B^*} = 5.325$ GeV (*short-dashed line*). (Adapted from Ref. [11].)

$$\xi(w) = \frac{2}{w+1} \exp \left[(1 - 2\rho^2) \frac{w-1}{w+1} \right], \quad \rho^2 = 1.53 \pm 0.36 \pm 0.14. \quad (117)$$

The evident agreement was possible because Ref. [11] did not employ the heavy-quark expansion of Eq. (71), in particular and especially not for the c -quark. The calculated result (*solid curve*) in Fig. 11 is well approximated by

$$\xi^{f_+}(w) = \frac{1}{1 + \tilde{\rho}_{f_+}^2 (w-1)}, \quad \tilde{\rho}_{f_+}^2 = 1.98. \quad (118)$$

Equations (111) were also used in Ref. [11] to extract $\xi(w)$ from $B \rightarrow D^*$. This gave $\xi^{A_1}(1) = 0.987$, $\xi^{A_2}(1) = 1.03$, $\xi^V(1) = 1.30$, an w -dependence well-described by Eq. (118) but with $\tilde{\rho}_{A_1}^2 = 1.79$, $\tilde{\rho}_{A_2}^2 = 1.99$, $\tilde{\rho}_V^2 = 2.02$, and the ratios, Eqs. (112), $R_1(1)/R_1(w_{\max}) = 1.08$, $R_2(1)/R_2(w_{\max}) = 1.06$.

This collection of results indicates the degree to which heavy-quark symmetry is respected in $b \rightarrow c$ processes. Combining them it is clear that even in this case, which is the nearest contemporary realisation of the heavy-quark symmetry limit, corrections of $\lesssim 30\%$ must be expected. In $c \rightarrow s, d$ transitions the corrections can be as large as a factor of two, as evident in Table 4.

5 Epilogue

This contribution provides a perspective on the modern application of Dyson-Schwinger equations (DSEs) to light- and heavy-meson properties. The keystone of this approach's success is an appreciation and expression of the momentum-dependence of dressed-parton propagators at infrared length-scales. That dependence is responsible for the magnitude of constituent-quark and -gluon masses,

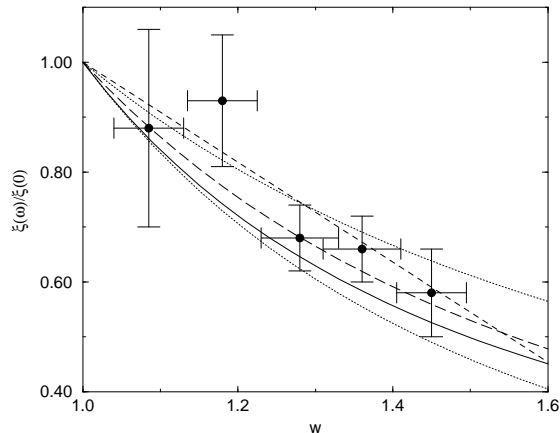


Fig. 11. Calculated [11] form of $\xi(w)$ (*solid line*) compared with experimental analyses: linear fit from Ref. [69], Eq. (116) (*short-dashed line*); nonlinear fit from Ref. [69], Eq. (117) (*long-dashed line*). The two lighter dotted lines are the nonlinear fit of Ref. [69] evaluated with the extreme values of ρ^2 : upper line, $\rho^2 = 1.17$ and lower line, $\rho^2 = 1.89$. The data points are from Ref. [74]. (Adapted from Ref. [11].)

and the length-scale characterising confinement in bound states; and is now recognised as a fact.

It has recently become clear that the simple rainbow-ladder DSE truncation is the first term in a systematic and nonperturbative scheme that preserves the Ward-Takahashi identities which express conservation laws at an hadronic level. This has enabled the proof of exact results in QCD, and explains why the truncation has been successful for light vector and flavour nonsinglet pseudoscalar mesons. Emulating more of these achievements with *ab initio* calculations of heavy-meson properties is a modern challenge.

However, at present, the study of heavy-meson systems using DSE methods stands approximately at the point occupied by those of light-meson properties seven – eight years ago. A Poincaré covariant treatment exploiting essential features, such as propagator dressing and sensible bound state Bethe-Salpeter amplitudes, has been shown capable of providing a unified and successful description of light- and heavy-meson observables. The goal now is to make the case compelling by tying the separate elements together; namely, relating the propagators and Bethe-Salpeter amplitudes via a single kernel. I am confident this will be accomplished, and the DSEs become a quantitatively reliable and intuition building tool as much in the heavy-quark sector as they are for light-quark systems.

While a more detailed understanding will be attained in pursuing this goal, certain qualitative results established already are unlikely to change. For example, it is plain that light- and heavy-mesons are essentially the same, they are simply bound states of dressed-quarks. Moreover, the magnitude of the b -quark's current-mass is large enough to sustain heavy-quark approximations for

its propagator and the amplitudes for bound states of which it is a constituent. In addition, and unfortunately in so far as practical constraints on the Standard Model are concerned, the current-mass of the c -quark is too small to validate an heavy-quark approximation.

Acknowledgments

I am grateful for the hospitality and support of my colleagues and the staff in the Bogoliubov Laboratory of Theoretical Physics at the Joint Institute for Nuclear Research, Dubna, Russia. This work was supported by: the Department of Energy, Nuclear Physics Division, under contract no. W-31-109-ENG-38; Deutsche Forschungsgemeinschaft, under contract no. Ro 1146/3-1; and benefited from the resources of the National Energy Research Scientific Computing Center.

References

1. C.D. Roberts and A.G. Williams, *Prog. Part. Nucl. Phys.* **33**, 477 (1994).
2. C.D. Roberts and S.M. Schmidt, *Prog. Part. Nucl. Phys.* **45**, S1 (2000).
3. R. Alkofer and L.v. Smekal, *Phys. Rept.* **353**, 281 (2001).
4. P. Maris and C.D. Roberts, “Dyson-Schwinger equations: A tool for hadron physics,” *nucl-th/0301049*.
5. P. Maris, C.D. Roberts and P.C. Tandy, *Phys. Lett.* **B 420**, 267 (1998).
6. P. Maris and C.D. Roberts, *Phys. Rev.* **C 56**, 3369 (1997).
7. P. Maris, A. Raya, C.D. Roberts and S.M. Schmidt, “Facets of confinement and dynamical chiral symmetry breaking,” *nucl-th/0208071*.
8. A. Bender, C.D. Roberts and L.v. Smekal, *Phys. Lett.* **B 380**, 7 (1996).
9. A. Bender, W. Detmold, C.D. Roberts and A.W. Thomas, *Phys. Rev.* **C 65**, 065203 (2002).
10. P. Maris and C.D. Roberts, “QCD bound states and their response to extremes of temperature and density.” In: *Proc. of the Wkshp. on Nonperturbative Methods in Quantum Field Theory, Adelaide, Australia, 2-13 Feb., 1998*, ed. by A.W. Schreiber, A.G. Williams and A.W. Thomas (World Scientific, Singapore 1998) pp. 132–151.
11. M.A. Ivanov, Yu.L. Kalinovsky and C.D. Roberts, *Phys. Rev.* **D 60**, 034018 (1999).
12. H.J. Munczek and A.M. Nemirovsky, *Phys. Rev.* **D 28**, 181 (1983).
13. C.H. Llewellyn-Smith, *Annals Phys. (NY)* **53**, 521 (1969).
14. H.J. Munczek, *Phys. Rev.* **D 52**, 4736 (1995).
15. R.W. Haymaker, *Riv. Nuovo Cim.* **14N8**, 1 (1991).
16. K.D. Lane, *Phys. Rev.* **D 10**, 2605 (1974); H.D. Politzer, *Nucl. Phys.* **B 117**, 397 (1976).
17. K. Langfeld, R. Pullirsch, H. Markum, C.D. Roberts and S.M. Schmidt, “Concerning the quark condensate,” *nucl-th/0301024*.
18. C.D. Roberts, “Continuum strong QCD: Confinement and Dynamical Chiral Symmetry Breaking,” *nucl-th/0007054*.
19. C. Alexandrou, P. De Forcrand and E. Follana, *Phys. Rev.* **D 65**, 117502 (2002); P.O. Bowman, U.M. Heller, D.B. Leinweber and A.G. Williams, *Phys. Rev.* **D 66**, 074505 (2002); and references therein.

20. J.C.R. Bloch, Phys. Rev. **D 64**, 116011 (2001).
21. R. Alkofer, C.S. Fischer and L.v. Smekal, Acta Phys. Slov. **52**, 191 (2002).
22. J. Skullerud and A. Kızılersü, JHEP **0209**, 013 (2002); J.I. Skullerud, P.O. Bowman, A. Kızılersü, D.B. Leinweber, A.G. Williams, “Nonperturbative structure of the quark-gluon vertex,” hep-ph/0303176.
23. J.C.R. Bloch, A. Cucchieri, K. Langfeld and T. Mendes, “Running coupling constant and propagators in SU(2) Landau gauge,” hep-lat/0209040.
24. P. Maris and P.C. Tandy, Phys. Rev. **C 60**, 055214 (1999).
25. L. Montanet, *et al.* [Part. Data Group Coll.], Phys. Rev. **D 50**, 1173 (1994); C. Caso *et al.* [Part. Data Group Coll.], Eur. Phys. J. **C 3**, 1 (1998).
26. P.O. Bowman, U.M. Heller and A.G. Williams, Phys. Rev. **D 66**, 014505 (2002).
27. K. Johnson, M. Baker and R. Willey, Phys. Rev. **136**, B1111 (1964).
28. M.S. Bhagwat, M.A. Pichowsky, C.D. Roberts and P.C. Tandy, “Analysis of a quenched lattice-QCD dressed-quark propagator,” nucl-th/0304003.
29. P. Maris, “Continuum QCD and Light Mesons.” In: *Wien 2000, Quark Confinement and the Hadron Spectrum — Proc. of the 4th Int. Conf., Vienna, Austria, 3-8 Jul 2000*, ed. by W. Lucha and K. Maung Maung (World Scientific, Singapore 2002) pp. 163-175.
30. M.B. Hecht, C.D. Roberts and S.M. Schmidt, “Contemporary Applications of Dyson-Schwinger Equations.” In: *Wien 2000, Quark Confinement and the Hadron Spectrum — Proc. of the 4th Int. Conf., Vienna, Austria, 3-8 Jul 2000*, ed. by W. Lucha and K. Maung Maung (World Scientific, Singapore 2002) pp. 27-39.
31. K.C. Bowler, *et al.* [UKQCD Coll.], Phys. Rev. **D 62**, 054506 (2000).
32. P.C. Tandy, “Covariant QCD modeling of light meson physics,” nucl-th/0301040.
33. P. Maris and P.C. Tandy, Phys. Rev. **C 61**, 045202 (2000).
34. P. Maris and P.C. Tandy, Phys. Rev. **C 62**, 055204 (2000).
35. P. Brauel, *et al.*, Z. Phys. **C 3**, 101 (1979).
36. S.R. Amendolia, *et al.* [NA7 Coll.], Nucl. Phys. **B 277**, 168 (1986).
37. J. Volmer, *et al.* [JLab F_π Coll.], Phys. Rev. Lett. **86**, 1713 (2001).
38. P. Maris, πN Newslett. **16**, 213 (2002).
39. C.D. Roberts, Nucl. Phys. **A 605**, 475 (1996).
40. P. Maris and C.D. Roberts, Phys. Rev. **C 58**, 3659 (1998).
41. G.R. Farrar and D.R. Jackson, Phys. Rev. Lett. **43**, 246 (1979).
42. G.P. Lepage and S.J. Brodsky, Phys. Rev. **D 22**, 2157 (1980).
43. M.S. Bhagwat, M.A. Pichowsky and P.C. Tandy, Phys. Rev. **D 67**, 054019 (2003).
44. S.R. Cotanch and P. Maris, Phys. Rev. **D 66**, 116010 (2002); P. Bicudo, Phys. Rev. **C 67**, 035201 (2003).
45. J. Praschifka, C.D. Roberts and R.T. Cahill, Phys. Rev. **D 36**, 209 (1987); C.D. Roberts, R.T. Cahill and J. Praschifka, Annals Phys. (NY) **188**, 20 (1988).
46. M. Bando, M. Harada and T. Kugo, Prog. Theor. Phys. **91**, 927 (1994).
47. R. Alkofer and C.D. Roberts, Phys. Lett. **B 369**, 101 (1996); B. Bistović and D. Klabučar, Phys. Lett. **B 478**, 127 (2000).
48. P. Maris and P.C. Tandy, Phys. Rev. **C 65**, 045211 (2002).
49. E.S. Ackleh, T. Barnes and E.S. Swanson, Phys. Rev. **D 54**, 6811 (1996).
50. G.S. Adams *et al.* [E852 Coll.], Phys. Rev. Lett. **81**, 5760 (1998). S.U. Chung *et al.*, Phys. Rev. **D 65**, 072001 (2002).
51. C.J. Burden, Lu Qian, C.D. Roberts, P.C. Tandy and M.J. Thomson, Phys. Rev. **C 55**, 2649 (1997).
52. C.J. Burden and M.A. Pichowsky, Few Body Syst. **32**, 119 (2002).
53. J.C.R. Bloch, Yu.L. Kalinovsky, C.D. Roberts and S.M. Schmidt, Phys. Rev. **D 60**, 111502 (1999).

54. M.A. Ivanov, Yu.L. Kalinovsky, P. Maris and C.D. Roberts, Phys. Lett. **B 416**, 29 (1998).
55. M.A. Ivanov, Yu.L. Kalinovsky, P. Maris and C.D. Roberts, Phys. Rev. **C 57**, 1991 (1998).
56. M. Neubert, Phys. Rep. **245**, 259 (1994); M. Neubert, "Heavy quark masses, mixing angles, and spin flavor symmetry." In: *The Building Blocks of Creation: From Microfermis to Megaparsecs, Boulder, Colorado, 6/Jun - 2/Jul 1993*, ed. by S. Raby and T. Walker (World Scientific, Singapore 1994) pp. 125-206; and references therein.
57. J.M. Flynn and C.T. Sachrajda, Adv. Ser. Direct. High Energy Phys. **15**, 402 (1998).
58. C. McNeile, "Heavy quarks on the lattice," hep-lat/0210026.
59. C.D. Roberts, Nucl. Phys. Proc. Suppl. **108**, 227 (2002).
60. Yu.L. Kalinovsky, K.L. Mitchell and C.D. Roberts, Phys. Lett. **B 399**, 22 (1997); C.R. Ji and P. Maris, Phys. Rev. **D 64**, 014032 (2001).
61. H. Munczek, Phys. Lett. **B 175**, 215 (1986); C.J. Burden, C.D. Roberts and A.G. Williams, *ibid* **285**, 347 (1992).
62. M.A. Pichowsky and T.-S.H. Lee, Phys. Lett. **B 379**, 1 (1996); M.A. Pichowsky and T.-S.H. Lee, Phys. Rev. **D 56**, 1644 (1997).
63. F.T. Hawes and M.A. Pichowsky, Phys. Rev. **C 59**, 1743 (1999).
64. G. Buchalla, A.J. Buras and M.E. Lautenbacher, Rev. Mod. Phys. **68**, 1125 (1996).
65. N. Isgur and M.B. Wise, Phys. Lett. **B 232**, 113 (1989); *ibid* **B 237**, 527 (1990).
66. The fitting used [25]: $V_{ub} = 0.0033$, $V_{cd} = 0.2205$, $V_{cs} = 0.9745$ and $V_{cb} = 0.039$; and, in GeV, $M_\rho = 0.77$, $M_{K^*} = 0.892$ and, except in the kinematic factor $\lambda(m_1^2, m_2^2, t)$ where the splittings are crucial, averaged D - and B -meson masses: $m_D = 1.99$, $m_B = 5.35$ (from $m_D = 1.87$, $m_{D_s} = 1.97$, $M_{D^*} = 2.01$, $M_{D_s^*} = 2.11$, and $m_B = 5.28$, $m_{B_s} = 5.37$, $M_{B^*} = 5.32$, $M_{B_s^*} = 5.42$). Furthermore, $b_0^u = 0.131$, $b_0^s = 0.105$, $b_3^u = 0.185 = b_3^s$ and $\epsilon = 10^{-4}$ were not varied, being instead fixed at the values determined in Ref. [67].
67. C.J. Burden, C.D. Roberts and M.J. Thomson, Phys. Lett. **B 371**, 163 (1996).
68. J.D. Richman and P.R. Burchat, Rev. Mod. Phys. **67**, 893 (1995).
69. J.E. Duboscq *et al.* [CLEO Coll.], Phys. Rev. Lett. **76**, 3898 (1996).
70. D.R. Burford, *et al.*, [UKQCD Coll.], Nucl. Phys. **B 447**, 425 (1995).
71. V.M. Belyaev, V.M. Braun, A. Khodjamirian and R. Rückl, Phys. Rev. **D 51**, 6177 (1995).
72. A. Anastassov *et al.* [CLEO Coll.], Phys. Rev. **D 65**, 032003 (2002).
73. W.R. Molzon *et al.*, Phys. Rev. Lett. **41**, 1213 (1978) [Erratum-*ibid.* **41**, 1523 (1978)]; S.R. Amendolia *et al.*, Phys. Lett. **B 178**, 435 (1986).
74. H. Albrecht *et al.* [ARGUS Coll.], Z. Phys. **C 57**, 533 (1993).